Front. Energy 2018, 12(1): 22–42
https://doi.org/10.1007/s11708-018-0541-7

REVIEW ARTICLE

Vishal TALARI, Prakhar BEHAR, Yi LU, Evan HARYADI, Dong LIU

Leidenfrost drops on micro/nanostructured surfaces

Abstract In the Leidenfrost state, the liquid drop is levitated above a hot solid surface by a vapor layer generated via evaporation from the drop. The vapor layer thermally insulates the drop from the heating surface, causing deteriorated heat transfer in a myriad of important engineering applications. Thus, it is highly desirable to suppress the Leidenfrost effect and elevate the Leidenfrost temperature. This paper presents a comprehensive review of recent literature concerning the Leidenfrost drops on micro/nanostructured surfaces with an emphasis on the enhancement of the Leidenfrost temperature. The basic physical processes of the Leidenfrost effect and the key characteristics of the Leidenfrost drops were first introduced. Then, the major findings of the influence of various micro/nanoscale surface structures on the Leidenfrost temperature were presented in detail, and the underlying enhancement mechanism for each specific surface topology was also discussed. It was concluded that multiscale hierarchical surfaces hold the best promise to significantly boost the Leidenfrost temperature by combining the advantages of both micro- and nanoscale structures.

Keywords Leidenfrost drop, Leidenfrost temperature, heat transfer enhancement, micro/nanostructured surfaces

1 Introduction

When a liquid drop is deposited on a highly superheated surface, fast vaporization at its bottom leads to the formation of a vapor layer that levitates the drop from the substrate. The hovering drop thus enters the Leidenfrost state, giving rise to a Leidenfrost drop [1]. Leidenfrost drops can be found in daily life occasions, for instance, professional chefs often sprinkle drops of water in a hot pan to make sure the utensil temperature is high enough before frying or sautéing food. They are also encountered in many engineering applications, such as spray cooling of nucleate reactors, spray quenching in metallurgy, liquid fire extinguishing, and fuel injection in combustion engines [2–6]. Since the vapor layer completely eliminates the liquid-solid contact, heat transfer between the drop and the solid substrate is merely via conduction and radiation through the vapor layer. Due to low thermal conductivity of the vapor, the Leidenfrost state represents a poor heat transfer regime with a minimal heat removal capacity. The surface temperature at which the Leidenfrost state commences, also known as the Leidenfrost point (LFP), demarcates the onset of film boiling, which is the least efficient mode of bulk boiling and is closely related to the critical heat flux (CHF) and the boiling crisis [7,8]. Therefore, it is of significant interest to suppress the Leidenfrost state (i.e., equally, to increase the LFP) for the benefit of enhancing heat transfer.

It has been long known that surface properties, including wettability, roughness and porosity, have substantial impact on the thermo-hydrodynamics of Leidenfrost drops. Traditionally, materials of different surface wetting characteristics were used to tailor the LFP [9–12]. It is observed that, as a general trend, rendering a material more hydrophilic defers the vapor layer formation/growth and reduces the possibility of departure from nucleate boiling (DNB) to film boiling, vice versa. While surface roughness can drastically alter surface wettability [13], its influence on the Leidenfrost effect is also tied to the recreation of liquid-solid contact by the roughness elements [8,14,15]. When the surface roughness increases, a thicker vapor layer is required to separate the liquid from the solid surface, thereby leading to a higher LFP. Recently, a myriad of surface engineering approaches enabled by surface chemistry and micro/nanofabrication have been devised to modulate the Leidenfrost phenomenon and tune the LFP. These approaches exploit micro-, nanoscale or hierarchical surface structures to alter one or more of the aforementioned physical parameters (wettability, roughness and porosity) [16].

The present article aims to provide a review of the recent

Received Sep. 27, 2017; accepted Dec. 15, 2017; online Feb. 8, 2018

Vishal TALARI, Prakhar BEHAR, Yi LU, Evan HARYADI, Dong LIU (✉)
Department of Mechanical Engineering, University of Houston, Houston, TX 77204-4006, USA
E-mail: dongliu@uh.edu

studies of suppressing the Leidenfrost state and elevating the LFP using micro/nanoengineered surfaces. The materials are organized as follows. First, the basic physics and theoretical background of the Leidenfrost effect are briefly described to set the context. Then, the Leidenfrost temperature enhancement with various micro/nanostructures on Leidenfrost surfaces will be presented. Finally, some conclusions will be drawn based on the general observations from the literature survey.

2 Background

2.1 Basic physical processes

When a liquid drop is gently deposited on a hot surface, it exhibits distinct hydrodynamic and heat transfer characteristics, depending on the wall superheat ΔT_{sat} (defined as $\Delta T_{sat} = T_s - T_{sat}$ where T_s is the surface temperature and T_{sat} is the saturation temperature of the liquid at the ambient pressure). As shown in Fig. 1, four heat transfer regimes can be identified as the wall superheat varies: film evaporation, nucleate boiling, transition boiling and film boiling [8,17,18]. At low ΔT_{sat}, heat is transferred by conduction from the wall to the liquid and evaporation takes place only along the liquid-gas interface. When ΔT_{sat} goes beyond the threshold for the onset of nucleate boiling, small bubbles will form inside the drop. If ΔT_{sat} is further escalated such that the corresponding wall heat flux exceeds the critical heat flux (CHF) condition, the drop will enter transition boiling. Eventually, the film boiling regime commences when T_s reaches the Leidenfrost temperature, or the Leidenfrost point (LFP). Subsequently, the drop is levitated from the surface by a thin vapor film generated by the rapid evaporation from the bottom of the drop, i.e., the liquid-solid contact is completely eliminated. Also shown in Fig. 1 is a plot of the lifetime (i.e., the evaporation time) of the drop, τ, as a function of ΔT_{sat}, in which τ reaches the maximum at the Leidenfrost temperature due to the insulating effect of the vapor layer. Afterward, the lifetime of the drop decreases as the evaporation becomes stronger owing to intensified conduction/radiation heat transfer through the vapor film at higher surface temperatures.

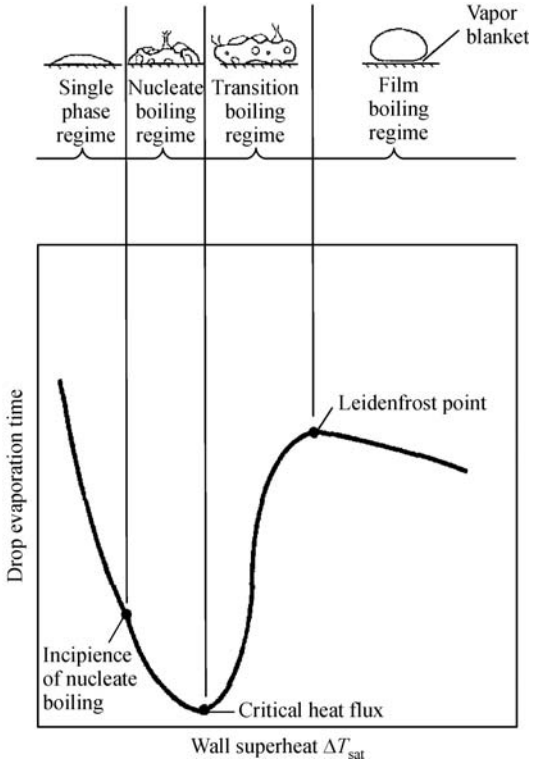

Fig. 1 Lifetime and heat transfer regimes of the drop at different wall temperatures (Adapted with permission from Bernardin and Mudawar [8])

2.2 Shape of Leidenfrost drops

Dynamics of the Leidenfrost drops are governed by the gravitational forces, surface tension forces, inertia forces and viscous forces. Consider a liquid drop with density ρ_L, surface tension σ, viscosity μ_L and initial radius R, the relative importance of the forces can be measured by the following non-dimensional numbers: ① the Bond number $\mathrm{Bo} = \rho_L g R^2/\sigma$, where g is the gravitational acceleration, ② the Reynolds number $\mathrm{Re} = \rho_L g(2R)U/\mu_L$, where U is the characteristic velocity, ③ the Capillary number $\mathrm{Ca} = \mu_L U/\sigma$, and ④ the Weber number $\mathrm{We} = \rho_L(2R)U^2/\sigma$. For sessile drops or drops that are deposited gently on the surface, the velocity U is so small that it is usually safe to assume $\mathrm{Re} \ll 1$, $\mathrm{Ca} \ll 1$, and $\mathrm{We} \sim 1$. Thus, the inertia and viscous effects are of secondary importance in the study of Leidenfrost drops concerned in this review. If the initial drop radius R is smaller than the capillary length λ ($\lambda = \sqrt{\sigma/\rho_L g}$, as an example, $\lambda = 2.5$ mm for water with $\rho_L = 960\,\mathrm{kg/m^3}$ and $\sigma = 0.059$ N/m), $\mathrm{Bo} \ll 1$, i.e., the effect of gravity is negligible with respect to surface tension. Since the Leidenfrost drop is completely non-wetting (due to the lack of liquid-solid contact), the drop will remain nearly spherical except at its bottom where it is slightly flattened, as shown in Fig. 2(a) [19]. Mahadevan and Pomeau [20] showed that the center of the pseudo-spherical drop will be lowered by owing to the deformation. Denoting the radius of the solid-vapor contact zone underneath the drop by l, it can be deduced that $l^2 \sim R\delta$ [21]. Further considering the change in the liquid-vapor interfacial surface area by the deformation, the increase in surface energy must be balanced by the decrease in the potential energy of the drop, i.e., $\rho_L g R^3 \delta \sim \sigma l^4/R^2$, which yields

$$l \sim R^2/\lambda. \tag{1}$$

In contrast, drops larger than λ become flattened by

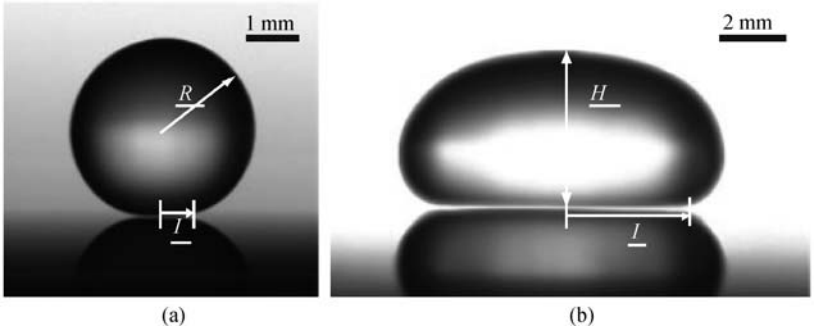

Fig. 2 Leidenfrost drop on a hot surface
(a) A quasi-sphere water drop; (b) a water puddle flattened by gravity (Adapted with permission from Quéré [19])

gravity as shown in Fig. 2(b), taking the form of a puddle of a constant thickness H. It can be shown that [22]

$$H \sim 2\sqrt{\sigma/\rho_{\mathrm{L}}g} = 2\lambda. \tag{2}$$

Further, using the volume conservation ($\pi l^2 H \sim 4\pi R^3/3$), the radius of the contact zone is

$$l \sim \sqrt{\frac{2}{3}} R^{3/2}/\lambda^{1/2}. \tag{3}$$

The drop geometries shown in Fig. 2 constitute the basic configurations of the Leidenfrost drops investigated in the literature.

2.3 Vapor layer below a Leidenfrost drop

The presence of a thin vapor film between the liquid drop and the solid surface is a key feature of the Leidenfrost drop. Thus, suppression of the Leidenfrost state centers on how to prevent/disrupt the formation of this dry vapor film and to reestablish the liquid-solid contact. For drops smaller than the capillary length ($R\langle\lambda$), the thickness of the vapor film, h, can be obtained by considering a truncated spheroidal drop of radius R as depicted in Fig. 3 [7,23]. Vapor evaporated from the bottom of the drop produces a lateral flow that provides the viscous pressure to levitate the drop against its weight. The classical analysis [7,23,24] yields

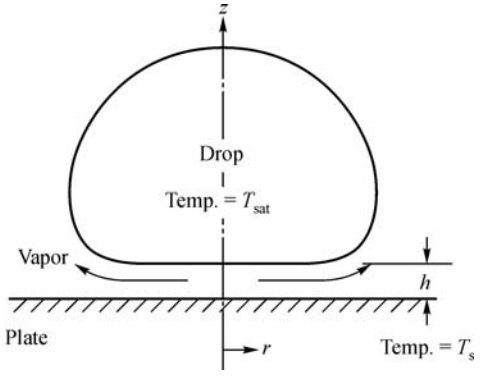

Fig. 3 Model of a levitated Leidenfrost drop

$$h = \left[\frac{9\mu_{\mathrm{v}}}{8h_{\mathrm{lv}}}\frac{k_{\mathrm{v}}\Delta T_{\mathrm{sat}}}{\rho_{\mathrm{v}}(\rho_{\mathrm{l}}-\rho_{\mathrm{v}})g}\right]^{1/4} R^{1/4}, \tag{4}$$

where μ_{v} and ρ_{v} are the viscosity and density of vapor, h_{lv} the latent heat of evaporation, and k_{v} the thermal conductivity of vapor. Later, Biance et al. [25] considered a general case that is applicable for both pseudo-spherical and puddle-shaped drops and derived the following results:

For small drops ($R < \lambda$),

$$h \sim \left[\frac{3k_{\mathrm{v}}\Delta T_{\mathrm{sat}}\rho_{\mathrm{L}}\mu_{\mathrm{v}}g}{4h_{\mathrm{lv}}\rho_{\mathrm{v}}\sigma^2}\right]^{1/4} R^{5/4}. \tag{5}$$

For puddles ($R > \lambda$),

$$h \sim \left[\frac{3k_{\mathrm{v}}\Delta T\mu_{\mathrm{v}}}{4h_{\mathrm{lv}}l\rho_{\mathrm{v}}\sigma g}\right]^{1/4} R^{1/2}. \tag{6}$$

Taking the typical values for different parameters involved, for instance, $k_{\mathrm{v}} \sim 0.03\,\mathrm{W/(m\cdot K)}$, $\mu_{\mathrm{v}} \sim 2 \times 10^{-5}$ Pa·s, $h_{\mathrm{lv}} \sim 10^6$ J/kg, $\rho_{\mathrm{v}} \sim 1\,\mathrm{kg/m^3}$, and $\rho_{\mathrm{L}} \sim 1000\,\mathrm{kg/m^3}$, Quéré [19] estimated that the vapor film thickness is on the order of 100 μm for a water Leidenfrost drop of a few millimeters in radius.

In most theoretical analysis, a uniform vapor thickness is assumed for the Leidenfrost drop for the sake of simplicity. However, in reality, the bottom surface of the drop is deformed into an inverted bowl shape due to the overpressure in the vapor layer. As shown in Fig. 4(a), the drop can be divided into an inner region and an outer region separated by the inner neck region [26]. The shape of the outer and inner regions is controlled by the balance of gravity and surface tension, whereas the neck region is set by the balance between viscous and surface tension forces. By using asymptotic analysis, the full shape of the drop can be constructed by matching the slopes and the curvature of the profiles at the boundaries on either side of the neck [26]. The computed drop shape is shown in Fig. 4(b). The concave depression of Leidenfrost drop was confirmed experimentally by Burton et al. [27] who measured the geometry of the vapor layer with laser

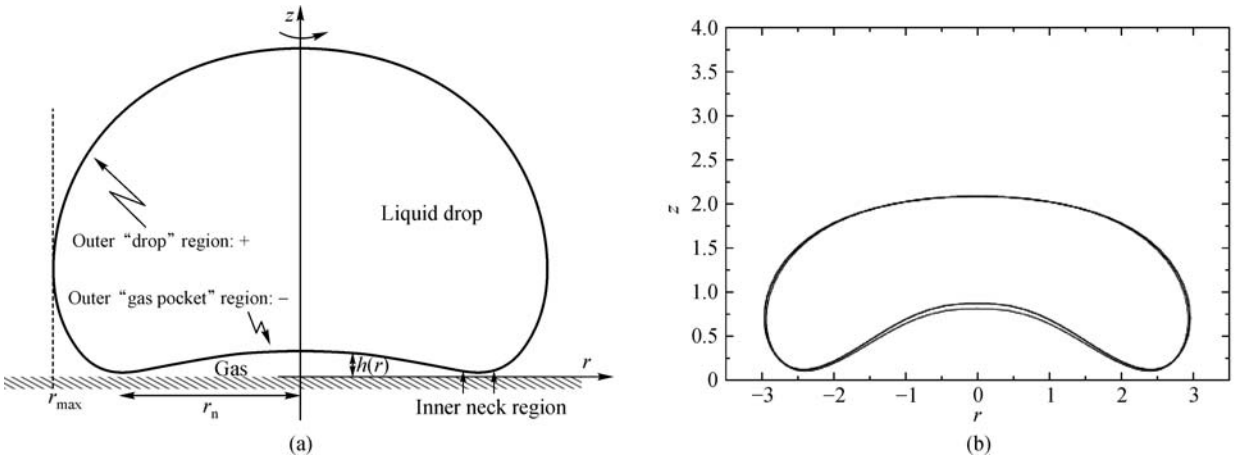

Fig. 4 Schematic cross section of a Leidenfrost drop with deformed bottom surface (Adapted with permission from Snoeijer et al. [26])

interferometry. It was further shown that the vapor layer geometry depends primarily on the drop size, not so much on the wall temperature and heat flux.

The stability of Leidenfrost drop also depends strongly on the initial drop size. For small drops, surface tension is able to maintain a static drop shape even in the presence of convection inside the drop, lateral vapor flow in the vapor layer as well as the Marangoni flow along the liquid-vapor interface [19,25]. However, for large drops, the vapor layer underneath the drop becomes unstable due to Rayleigh-Taylor instability. As a consequence, one or more bubbles rise from the center of the puddle and burst through the upper interface, turning the drop into a torus, as shown in Fig. 5. Biance et al. [25] showed that the threshold drop radius without the bubble formation is $R_c = 1.92H \approx 4\lambda$, which translates to $R_c \approx 1$ cm for a water drop. Moreover, self-sustained, star-shaped interfacial oscillations were observed for the Leidenfrost drops, as shown in Fig. 6 [28–31]. These oscillations were postulated to be driven by capillary waves that are generated by the large shear stress at the liquid-vapor interface.

2.4 Leidenfrost temperature

As discussed in Section 2.1, the Leidenfrost temperature demarcates the phenomenological boundary between the transition boiling regime and the film boiling regime. Both static and dynamic Leidenfrost temperatures have been considered. The static Leidenfrost temperature is determined by the drop lifetime method, in which the evaporation time of a sessile drop of a given initial volume is measured over a range of temperatures on a heated surface and the LFP is defined as the surface temperature corresponding to the longest evaporation time (as depicted in Fig. 1) [32]. Alternatively, the dynamic Leidenfrost temperature is used as the threshold to distinguish the hydrodynamic behavior of an impinging drop in contact boiling from that in film boiling, as shown in Fig. 7. In contact boiling, partial liquid-solid contact persists, and the drop spreading on the wall is accompanied by typical nucleate boiling characteristics (including bubble nucleation and growth) at the wetted area. In contrast, the stable thin vapor layer in film boiling causes the drop to bounce

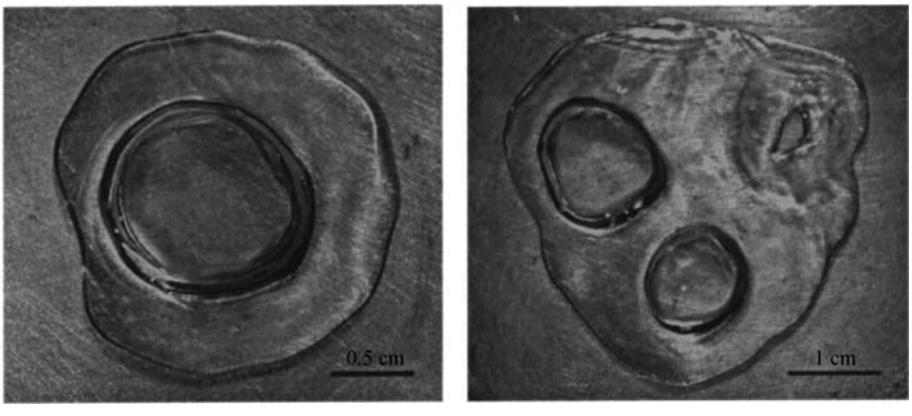

Fig. 5 Vapor bubble (s) rising from the center of large puddles of water (Adapted with permission from Biance et al. [25])

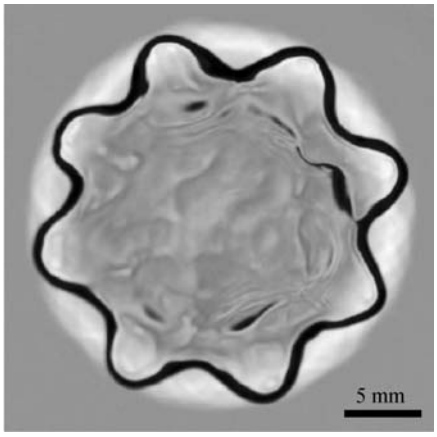

Fig. 6 Self-sustained, star-shaped oscillations of Leidenfrost drop (Adapted with permission from Ma et al. [31])

without shattering and completely prevents the liquid-solid contact [33–35]. The dynamic Leidenfrost temperature is usually higher than its static counterpart [35].

Due to the poor heat transfer associated with film boiling, the LFP forebodes the minimum heat flux (MHF) condition that is unfavorable in many practical applications, such as cooling of nucleate reactors and spray quenching in material processing [36–38]. Thus, it is crucial to delineate the influence of the material properties and the process parameters on the LFP for the sake of effective enhancement strategies. Two comprehensive reviews by Bernardin and Mudawar [8] and Liang and Mudawar [39] reveal that the liquid mass and drop size, liquid properties, liquid's initial subcooling, the thermal properties of the solid wall, surface finish, the ambient pressure as well as the method of liquid deposition on the surface all affect the LFP, although discrepancies often exist with regard to the trend and degree of the effects. The overall assessment was that the liquid mass, liquid subcooling, dissolved gas and solid thermal properties only marginally influence the Leidenfrost temperature, whereas increasing ambient pressure, surface wettability or drop impact velocity shows more positive correlation. Particularly, it was found the surface conditions, such as surface roughness and porosity, have strong influence on the LFP. Lately, this surface dependence has become the central theme of micro/nano-enabled Leidenfrost enhancement technologies, and the recent development will be discussed in great detail in the following sections.

In the meanwhile, a myriad of theoretical models have been postulated to predict the LFP for sessile drops and the minimum film boiling point for pools of liquid. As summarized by Bernardin and Mudawar [8], some of the key theories include: the hydrodynamic instability model [40,41] that was built on the Taylor instability analysis of the liquid-vapor interface of the vapor layer; the metastable liquid-mechanical stability model [42,43] that connected the Leidenfrost state to the superheat limits of homogeneous or heterogeneous nucleation; the thermomechanical non-equilibrium model [44] that extrapolated the flow boiling model for a vertical dryout flow condition to the LFP, and the wettability model [45,46] that explored the temperature-dependence of contact angle or the viability of surface adsorbed liquid precursor film. Subsequently, the same authors also proposed a cavity activation model that attributed the formation and stability of the vapor layer to the activation and growth of bubbles in the microscopic cavities on the surface [47]. However, the existing models either suffer from unsupported hypothesis or lack robustness when applied to predict the

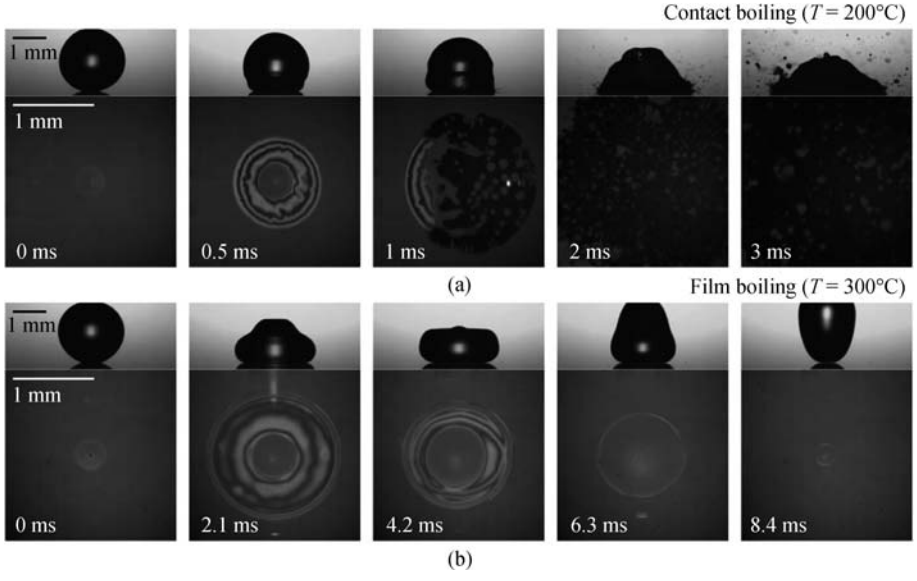

Fig. 7 Contact boiling vs. film boiling of an impinging drop (Adapted with permission from Tran et al. [33])

LFP for a wider range of fluids and surface conditions. Therefore, new physics-based models are called for to fully elucidate the mechanisms of the Leidenfrost phenomenon, especially, on complex micro/nanostructured surfaces. In the present review, the underlying physics associated with each LFP enhancement surface topology will be discussed whenever possible.

3 Leidenfrost drop on micro/nanoengineered surfaces

In the Leidenfrost state, the liquid drop is insulated from the solid surface by a vapor layer. The persistent absence of liquid-solid contact constitutes the main cause for deteriorated heat transfer performance in spray cooling and pool boiling at temperatures beyond the LFP. Thus, various micro/nanoscale surface structures have been devised to disrupt the liquid-vapor interface or to evacuate the vapor phase in order to diminish the envelope of the film boiling regime. The engineered surface structures are of different topographical configurations, but they can be broadly classified into two groups: pillar structures and porous structures. The former group aims primarily to modify the surface roughness, and the latter group to tailor the surface porosity. Together with the textural modification, the surface structures can be further treated chemically to become super hydrophobic or super hydrophilic with the general understanding that a hydrophilic material defers the vapor layer formation [9–12]. In the following, the hydrodynamic and heat transfer characteristics of Leidenfrost drops on these two groups of micro/nanostructured surfaces will be reviewed, respectively.

3.1 Effect of pillar structures on the Leidenfrost temperature

Modifying surface roughness is known to have a significant impact on surface wettability and the number density of nucleation sites in pool boiling [48,49]. For the Leidenfrost phenomenon, it was generally agreed that when the surface roughness increases, the protruding surface elements help to sustain the liquid-solid contact as they penetrate into the vapor film requiring a thicker vapor layer to separate the liquid from the solid surface [8,14,15,50]. Traditionally, only random surface roughness had been introduced to raise the LFP via particle/sand blasting [50,51], particle coating [52], and salt deposition [53–55]. Although effective, the exact effect of these random surface textures on the LFP is difficult to quantify as they tend to modify multiple surface parameters, such as the roughness profile, wettability and porosity, at the same time. Only till recently, patterned micro/nanopillar arrays can be fabricated on the Leidenfrost surfaces to allow fine control over the geometric parameters (shape and dimensions) of the roughness structures. Hence, accurate relationship can be established between the surface topology and the LFP of the drop.

3.1.1 Micropillar structures

The micropillars can be fabricated by standard lithography technique or femtosecond laser surface processing and are usually arranged in a square array. The profile of a typical micropillar structure is characterized by the height, the width and the interspacing of the roughness elements, as shown in Fig. 8(a).

Kim et al. [56] presented one of the first studies on the effect of microstructures on the Leidenfrost phenomenon by using micropillars (shown in Fig. 9(a)). The LFP on smooth silicon surface was compared to that on the surface with 15-μm high cylindrical micropillar arrays. The surface wettability was controlled by the deposition of gold (Au) and silicon oxide (SiO_2).The results in Fig. 9(b) show that the LFP increases from 264°C and 274°C for the flat Au- and SiO_2-coated surfaces to 290°C and 325°C for surfaces decorated with micropillars, respectively. The LFP enhancement was ascribed to the intermittent liquid-contact contact induced by the presence of micropillars that bridge the droplet to the solid surfaces (depicted by white arrows in Fig. 9(c)). By estimating the relative magnitude of the pillar height to the vapor film thickness, this study confirms the first-order effect of micropillars on the LFP enhancement is to re-initiate the liquid-solid contact.

Elevation of the LFP on micropillar structures was also reported by Kwon et al. [57]. As shown in Fig. 10(a), square micropillar arrays were fabricated on a silicon substrate with a fixed width of $a = 10$ μm and a height of 10 μm, but the edge-to-edge spacing b was varied between 3.3 μm to 100 μm. It was discovered that the micropillar structure affects the drop dynamics, and the increase in LFP is higher on surfaces with sparser rather than denser spacing. Figure 10(b) exemplifies that as the pillar spacing increases from 20 μm to 100 μm, the LFP increases proportionally from 270°C to 370°C. This finding is quite counter-intuitive since it is expected that denser pillar structure would facilitate liquid wetting due to stronger capillary effect and, hence, further enhance the LFP. The discrepancy was explained by a hypothesis that the presence of micropillar arrays not only increases the capillary force to maintain the liquid-solid contact, but also impedes the outward vapor flow escaping through the gap under the drop, which generates the compressive pressure force levitating the drop (Fig. 10(c)). Thus, the LFP enhancement depends on the competition of these two mechanisms. Similar conclusions were reached in a work by Feng et al. [58], where the dependence of the LFP on the micropillar size and the solid area ratio f ($f = a^2/[a^2 + (a+b)^2]$) was investigated and the LFP was found to decrease with increasing f.

While the foregoing studies suggest the LFP will be

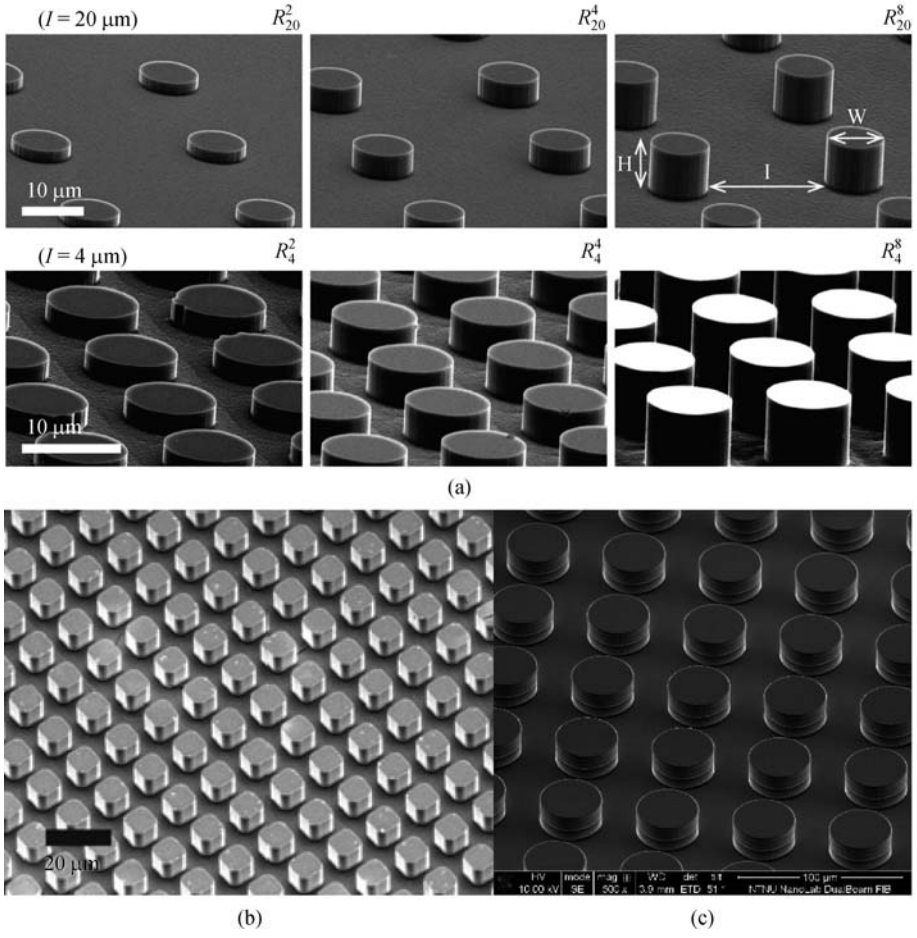

Fig. 8 Patterned micropillar arrays for Leidenfrost drops (Adapted with permission from (a) Tran et al. [33], (b) Kwon et al. [57] and (c) Park et al. [60])

augmented by the micropillar structures, Arnaldo del Cerro et al. [59] observed the reduction of LFP on patterned metallic surfaces with pillar-like structure (designated by *p*) and hole array structure (designated by *h*), as shown in Fig. 11(a). The spacing between neighboring pillars was remained as 17 μm and the pillar height was varied between 3 μm to 9 μm. Figure 11(b) indicates the Leidenfrost state commences at about 140°C–160°C on both microstructured surfaces, significantly below the LFP on a flat surface. By viewing the pillar-like structure as interconnected microcavities, the LFP reduction was postulated to stem from the quick formation and growth of bubbles from these cavities [47] that merge into a bubble network, although not a stable vapor film, to counteract the pressure of the droplet. The validity of this study is somewhat shadowed by how the LFP was determined, i.e., instead of using the conventional lifetime method, the LFP was identified as the temperature at which the droplet does not experience sudden boiling and the contact angle exhibits an abrupt increase. Further, due to the constraints of the laser machining technique, the shape and geometry of the micropillar structure in Ref. [59] cannot be controlled accurately.

These drawbacks were overcome by Tran et al. [34] in an investigation on the dependence of the dynamic LFP on micropillar height, pitch and the drop impact velocity. In this work, the micropillars have a sharp profile as shown in Fig. 8(a). The pillar width was kept constant (9 μm), while the height was varied as 2 μm, 4 μm and 8 μm, respectively, and the interspacing 4 μm and 20 μm. Figure 12 illustrates that for a given spacing, the LFP decreases drastically when the pillar height increases from 2 μm to 8 μm. For instance, it is reduced by 50 K for $6 \leqslant We \leqslant 270$ and nearly 100 K for $10 \leqslant We \leqslant 890$ compared to the smooth surface, where We is defined using the drop diameter and the impact velocity. It was suggested that the reduction in LFP with respect to the pillar height may be caused by two effects: ① a larger height yields the increase in the total surface area available for heat transfer, which lowers the temperature differential (defined as the difference between the LFP and the saturation temperature of the liquid) required to maintain a stable vapor film; ② the outward flow of vapor generated under the drop is obstructed by the pillars and the buildup of vapor pressure

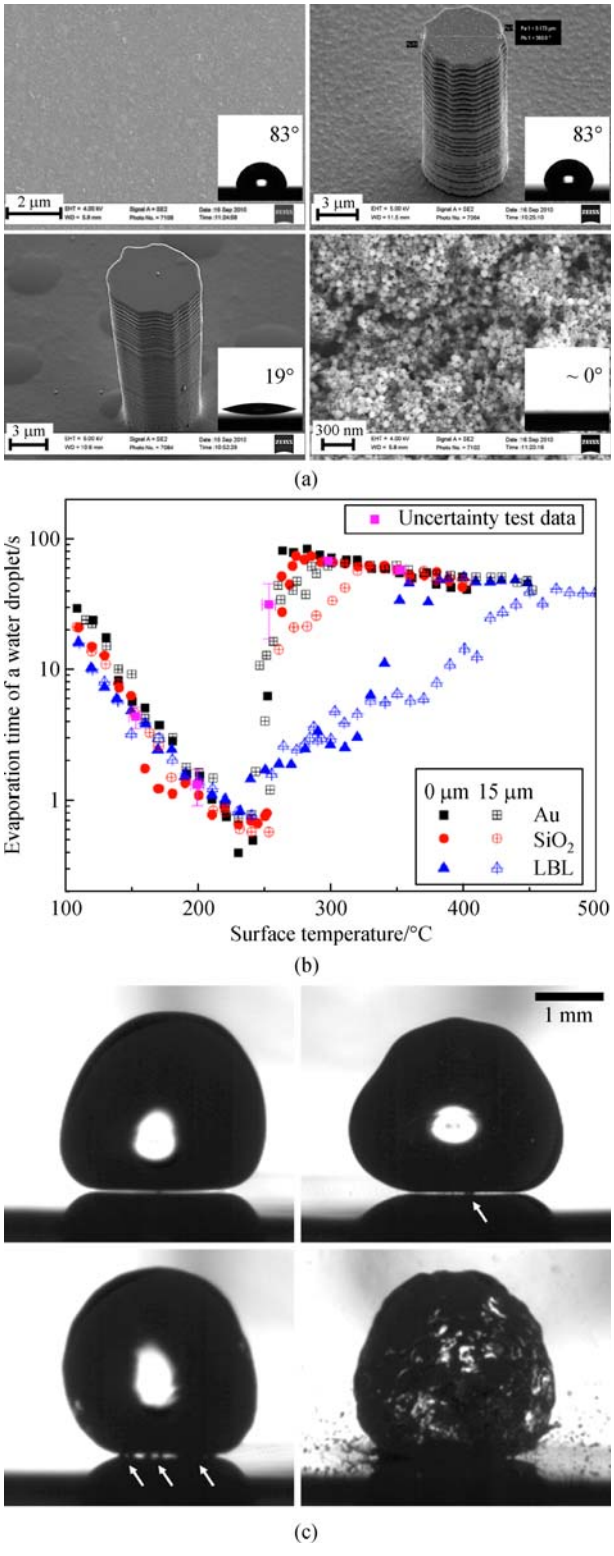

Fig. 9 The effect of surface roughness height, wettability and nanoporosity on the LFP (Adapted with permission from Kim et al. [56])

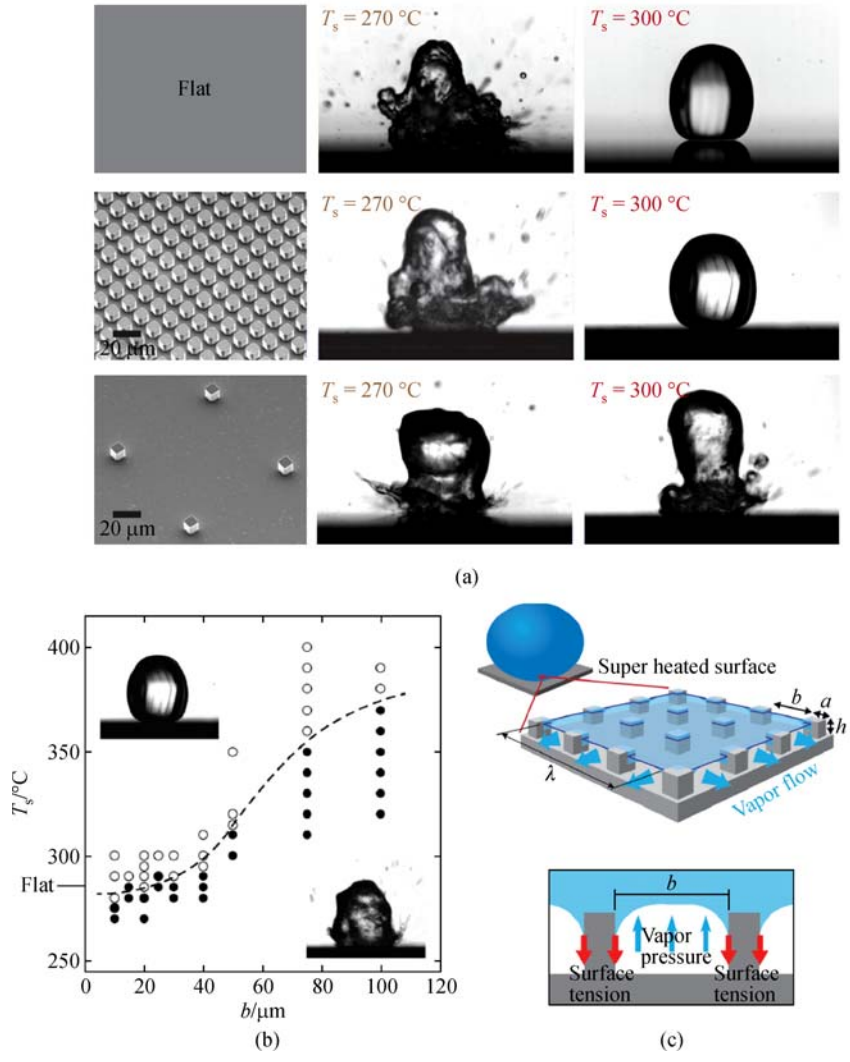

Fig. 10 Effects of micropillar structures with different edge-to-edge spacing on drop dynamics and the LFP (Adapted with permission from Kwok et al. [57])

makes it possible to support the drop even at a lower surface temperature.

In view of the aforementioned results, some in consistencies seem to exist regarding the effect of micropillar structures on the Leidenfrost temperature. The situation is further complicated by a recent study by Park et al. [60] for square arrays of cylindrical micropillar (shown in Fig. 8(c)). In this work, all three geometrical parameters of the pillars (the width, height and pitch) were varied, and both the static and dynamic Leidenfrost temperatures were measured. The results in Fig. 13(a) and (b) show the LFP increases with the pitch size but decreases with the width. The trend is consistent with the finding in Ref. [57] since a larger pitch or a smaller width corresponds to a greater edge-to-edge spacing. When comparing the LFPs on the flat surface and the microstructured surface in Fig. 13(c), however, a dispersion can be noticed: the LFP can be either raised or reduced, depending on the width, the pitch-to-width ratio and the height-to-width ratio. A scrutiny reveals that the static LFP is almost always enhanced whereas the modulation of the dynamic LFP can go in both directions.

In addition to the typical micropillar structures, a microrib-patterned super hydrophobic surface was also developed by Hays et al. [61] to study the influence of topography on droplet-substrate heat transfer of sessile water droplets. The microrib-cavity structure depicted in Fig. 14 is characterized by the cavity fraction, defined as the relative projected area not occupied by the microribs to total surface area. It was found that increasing the cavity fraction delays the onset of nucleate boiling and decreases the Leidenfrost temperature. If the cavity fraction is increased enough, nucleate boiling is suppressed at all surface temperatures and the Leidenfrost drop behavior occurs near the classical critical heat flux point. This change may be explained by the presence of persistent

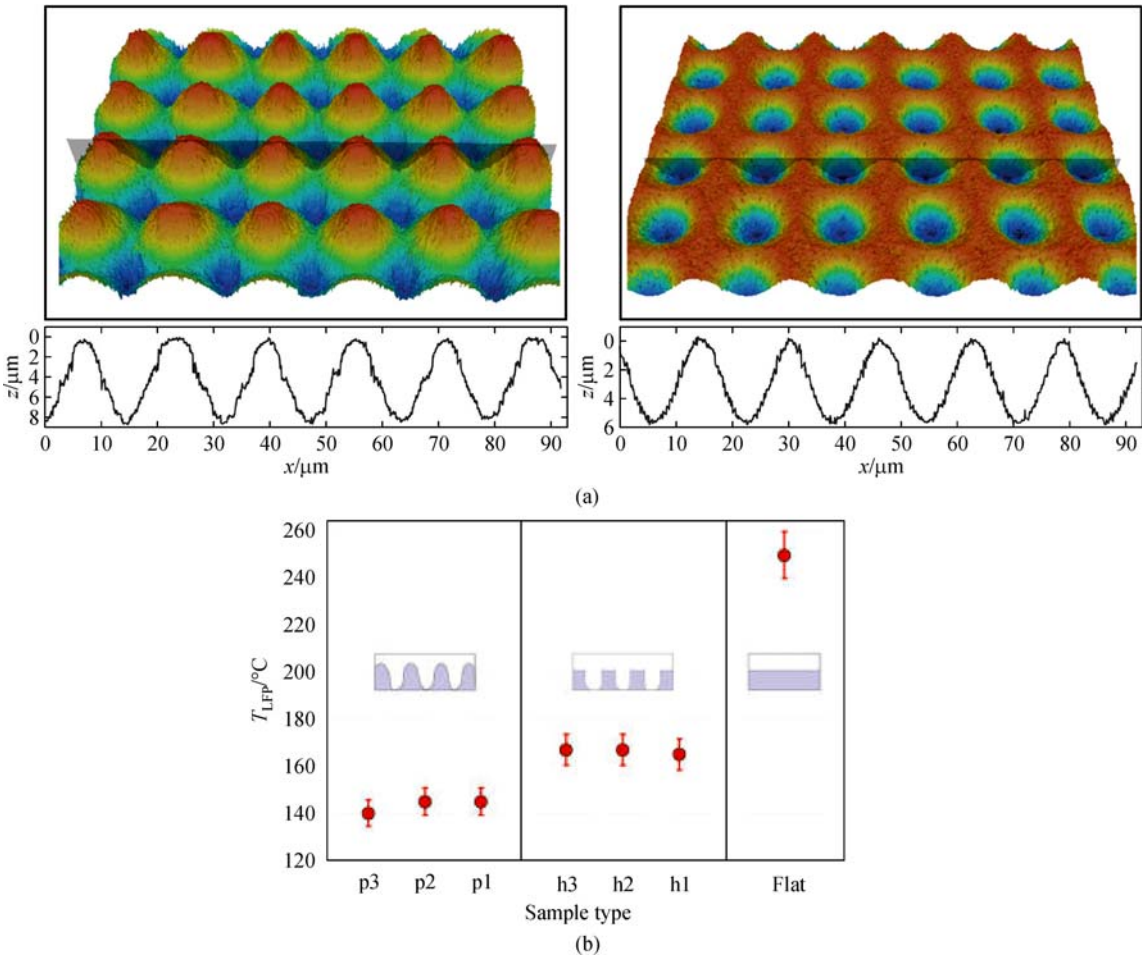

Fig. 11 Microstructures generated by a picosecond pulsed laser source
(a) Pillar-like and hole arrays; (b) LFP measurement (Adapted with permission from Arnaldo del Cerro et al. [59])

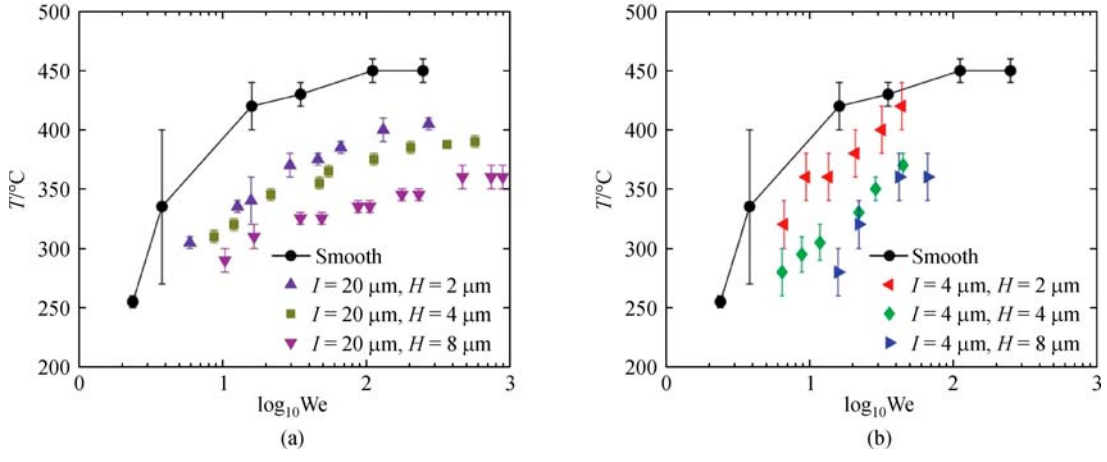

Fig. 12 The dependence of dynamic LFP on micropillar height, interfacing and Webber number (Adapted with permission from Tran et al. [33])

vapor cavities on the microstructured surfaces that act to stabilize the vapor film beneath the boiling droplet at lower supercritical temperatures.

3.1.2 Nanopillar structures

The term “nanopillar” is used loosely in this review to refer

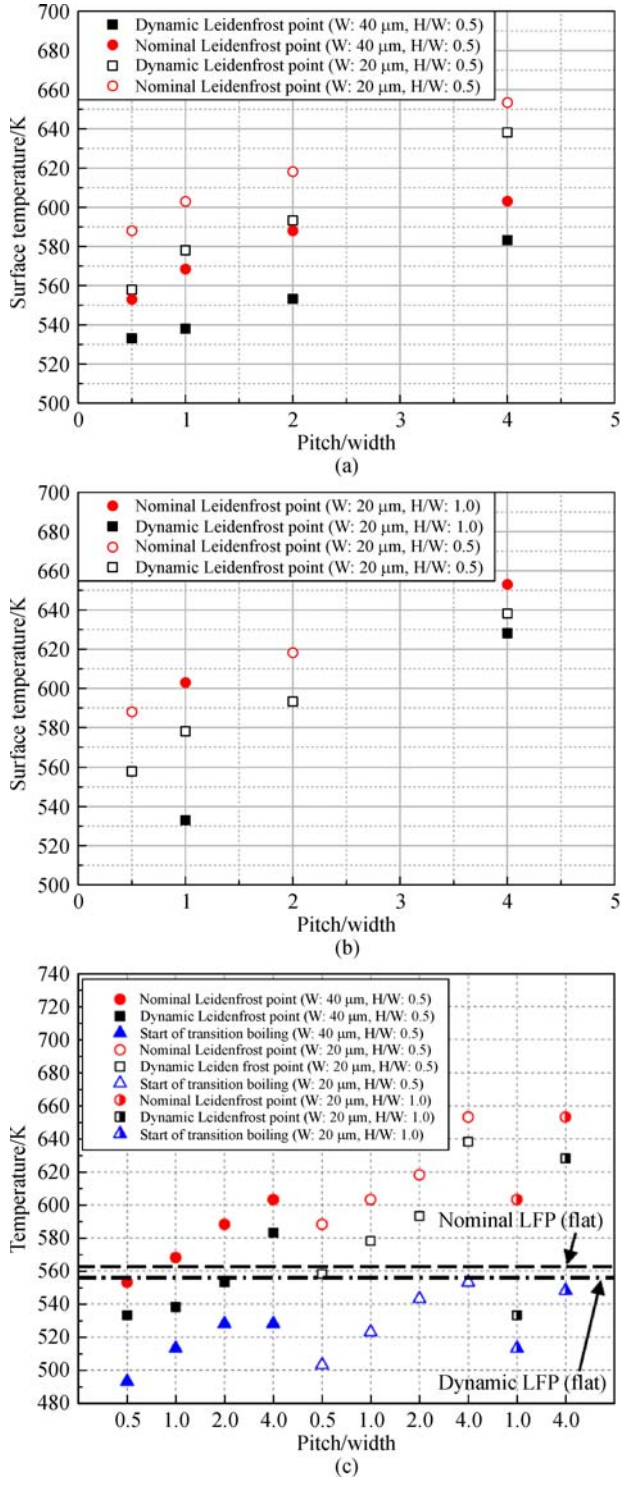

Fig. 13 The dependence of Leidenfrost temperature on micropillar geometries (Adpated with permission from Park et al. [60])

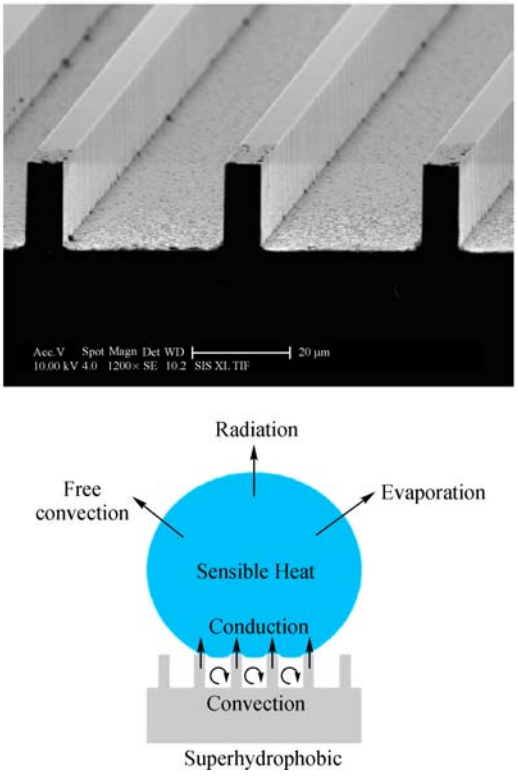

Fig. 14 SEM of the microrib patterns and the corresponding heat transfer mechanisms on the microstructured surface (Adapted with permission from Hays et al. [61])

to any nanoscale surface structures that are extruding out of the substrateplane, such as nanofibers, nanotubes and nanowires, etc. These nanopillars are known for their tunable morphology, e.g., the diameter can be controlled from a few to hundreds of nanometers and the height from a few micrometers to millimeters. Thus, they can be exploited to modulate the surface area, roughness and porosity of a solid substrate [62]. The extruding nanopillars can modify the surface porosity because, when fabricated in arrays, the standalone nanopillars are often entangled into bundles to form an interconnected nanoporous or microporous layer. The nanopillar-covered surface usually exhibits super hydrophilic wetting characteristics, featured by excellent liquid spreading. The nanoporosity also leads to strong capillary wicking allowing liquid to penetrate into the nanopillar layer. In addition, the microscale pores and/or fabrication defects can act as nucleation sites to precipitate nucleate boiling at the liquid-solid contact.

Weickgenannt et al. [63,64] and Sinha-Ray et al. [65] presented the early work on using polymer nanofibers to enhance the efficiency of spray cooling and suppress the Leidenfrost effect. PAN [poly (acrylonitrile)] nanofibers were electrospun on stainless steel foil to form a layer of nonwoven nanofibers mat with a pore size of ~1 μm (shown in Fig. 15). Liquid imbibition into the inter fiber pores results in spontaneous spreading of the impacting drop over a wider wetting area that helps to suppress the liquid atomization and promote evaporation. It was also hypothesized that vapor can escape partially or completely through the inter fiber pores. However, no direct measurement of the LFP was reported. Nair et al. [62] studied the

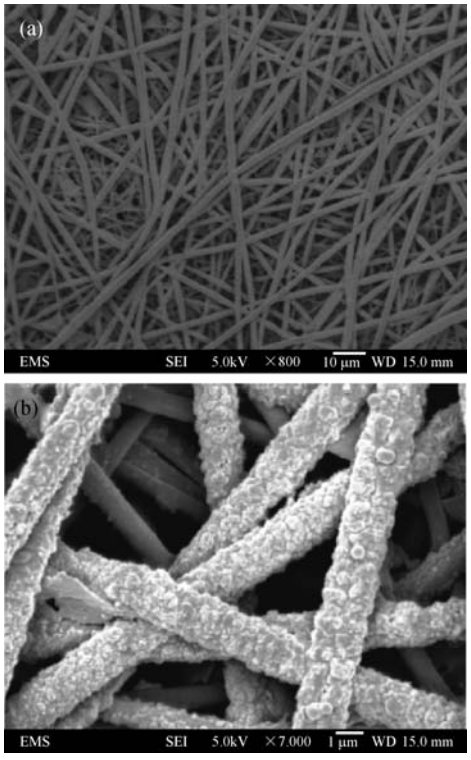

Fig. 15 SEM images of the polymer nanofiber mat and the single nanofibers (Adapted with permission from Sinha-Ray et al. [65])

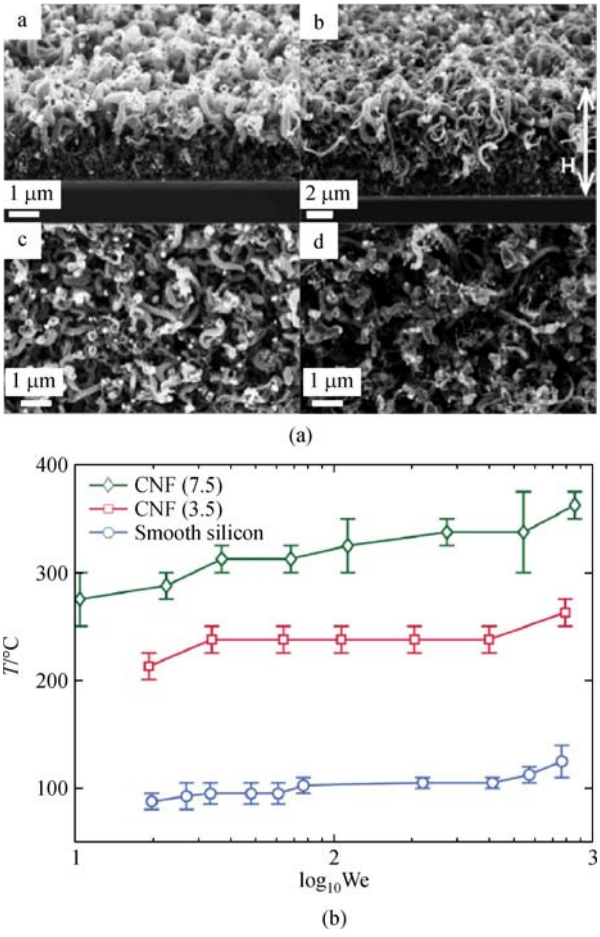

Fig. 16 Study of LFP on CNF nanostructures
(a) Morphology of the CNF layers; (b) LFP for smooth silicon surface and CNF-covered surfaces (Adapted with permission from Nair et al. [62])

Leidenfrost temperature increase for FC-72 droplets impacting on carbon nanofiber (CNF)-covered surfaces. The CNFs have an average diameter of 127 nm. Depending on the synthesis time, the CNF length (i.e., the thickness of the CNF layer) can be varied from 3.4 μm to 7.5 μm (shown in Fig. 16(a)). The corresponding porosity was 0.76 and 0.86, respectively. By observing the droplet impact dynamics in the transition from contact boiling to film boiling, it was found the dynamic LFP was higher on the CNF surfaces than on the smooth silicon surface, and increasing the fiber length causes the LFP to increase considerably (depicted in Fig. 16(b)). The latter observation is in stark contrast with the previous finding that the LFP is inversely correlated with the pillar height on surfaces covered by micropillar structures [34]. The analysis of the relevant time scales (including the time for the CNF temperature to cool, the time for the CNF to be exposed to the vapor flow and the time for heat to conduct from the silicon substrate) suggests that due to the small scale of the CNFs, they are cooled by the vapor flow before the liquid impact, thus extending the contact boiling range to a much higher temperature than on smooth and microstructured surfaces.

Kim et al. [66] investigated the effect of zirconium nanotubes on the dynamics and the LFP of water droplet. The nanotube arrays consist of individual nanotubes with 20 nm diameter and 2.5 μm height and the nanotube surface has a measured contact angle of 4.2°, as shown in Fig. 17(a). Due to nanotube-induced liquid spreading and absorption, the LFP increases from 300°C on the bare surface to 370°C on the nanotube-grown surface (Fig. 17(b)). In the transient region between 300°C and 370°C, explosion-like dynamics with violent ejection of sub-droplets was observed for the water droplet. This was attributed to the vigorous nucleate boiling occurring at nucleation sites created from the pores in the nanotube arrays. As depicted in Fig. 17(c), a slip condition was postulated at the solid surface because of the porous feature of the nanotube arrays. Consequently, the vapor evaporated from under the droplet can escape with less resistance, leading to higher surface temperature to trigger the "cannot-touch-the-wall condition."

Nanowires have also been employed to shift the LFP and control the directional motion of droplets. One example is the work by Auliano et al. [67] who conducted Leidenfrost experiments on a silicon surface covered with silicon nanowires. Figure 18(a) shows that microscale crevices

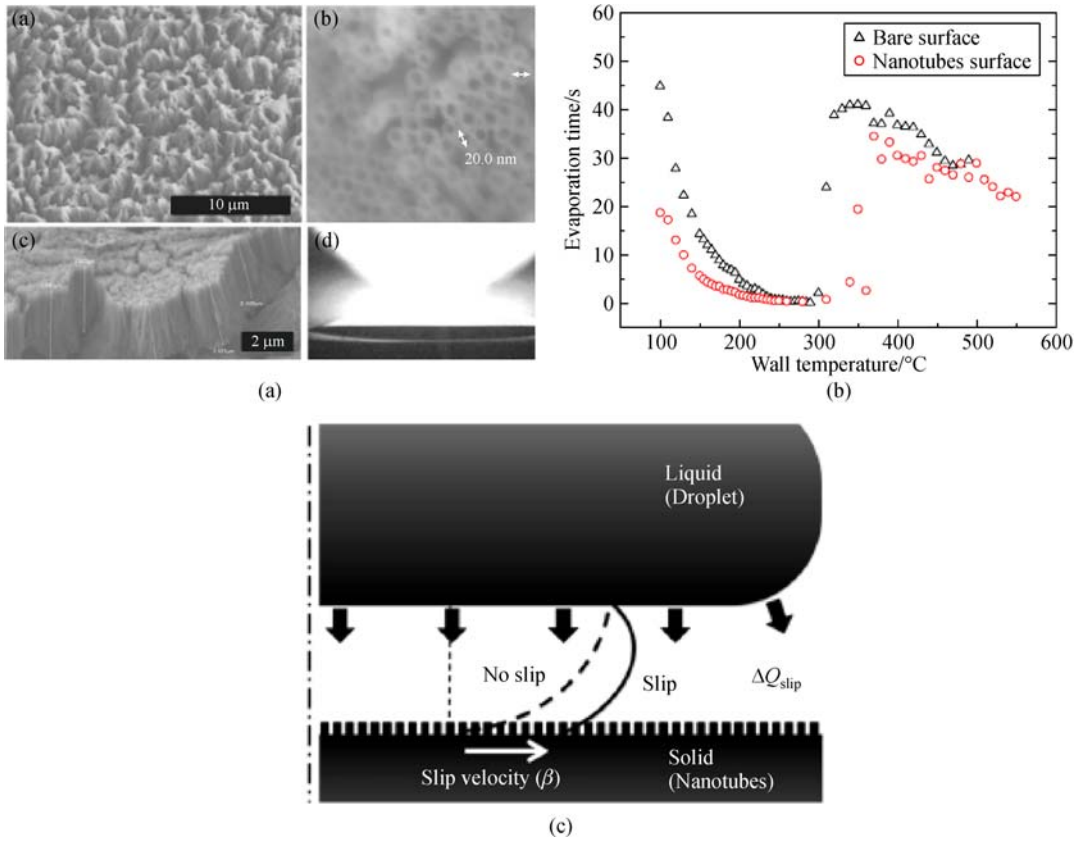

Fig. 17 Zironium nanotube surface and the impact on LFP (Adapted with permission from Kim et al. [66])

were created due to the bundling of nanowires during the fabrication process, which would act as nucleation sites for bubble formation. In the meanwhile, the porosity of the nanowire arrays induces strong capillary wicking effect. Consequently, the LFP was found to increase significantly on nanowire-covered surfaces than on the smooth silicon surface, and the increment is proportional to the height of the nanowires (Fig. 18(b)). In another study, Agapov et al. [68] explored the use of tilted silicon nanopillars (460 nm tall) in guiding the unidirectional movement of Leidenfrost droplets. Although the LFP was not their focus of interest, they generated phase diagrams to delineate the transition from contact boiling to film boiling of the droplet at different Weber numbers. The comparison shows the LFP is elevated on the surface with tilted nanopillar arrays.

3.1.3 Hierarchical micro/nanoscale structures

From the foregoing discussions, it becomes apparent that microscale and nanoscale surface structures play different roles in affecting the Leidenfrost phenomenon. By penetrating into the vapor layer, the microstructures can re-initiate the liquid-solid contact and restore film boiling to contact boiling. However, the configuration and dimensions of the microstructures must be chosen carefully to balance the competition between the microstructure-induced capillary wetting and the obstruction to the vapor escaping pathway. Furthermore, there are evidences showing that the microstructures can adversely deteriorate the LFP since excessive amount of vapor may be generated owing to the enlarged heat transfer area by the microstructures. On the other hand, nanoscale structures seem to be utterly beneficial to the LFP enhancement: they promote liquid spreading, enable capillary wicking, and even provide nucleation sites when manufacturing defects are present or the nanostructures are entangled during the fabrication process. Therefore, it is very appealing for greater LFP improvement if the advantages of both the microscale and the nanoscale surface structures can be garnered collectively, i.e., via micro/nanoscale hierarchical structuring.

Such endeavors are ample in the literature. Kim et al. [56] found that if the Leidenfrost surfaces are coated with a nanoporous layer (about 600 nm thick) made of SiO_2 nanoparticles (23 nm in average diameter), explosive heterogeneous boiling will ensue at the bottom of the droplet once the intermittent liquid filaments are established by the micropillars. The velocity of the vapor generated can exceed the critical velocity of the Kelvin-Helmholtz instability. When this occurs, the liquid-vapor interface is severely disrupted, resulting in violent splashes of tiny sub-droplets that prevent the formation of a stable

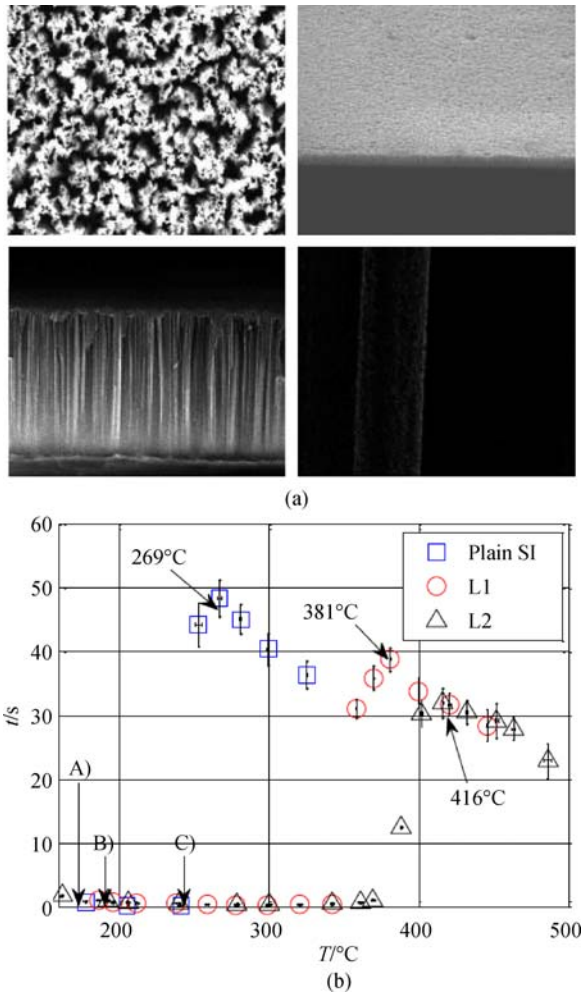

Fig. 18 Study of LFP on silicon nanowire-coated surface (a) SEM of silicon nanowires; (b) Leidenfrost temperature measurements (Adapted with permission from Auliano et al. [67])

vapor film. Accordingly, the LFP on the nanoporous surfaces with micropillars increases to as high as 453°C (shown in Fig. 9(b)), comparable to the superheat limit. Kwon et al. [57] further recognized that the Leidenfrost phenomenon is governed by the downward capillary wetting force and the upward vapor compressive pressure, and the wetting depends on the smallest texture length scale whereas the vapor pressure on the largest texture length scale. Based on this physical insight, they devised a hierarchical texture surface by spin-coating 220 nm diameter silica nanoparticles on the micropillar arrays (Fig. 19), which increases the capillary pressure without increasing the resistance to the escaping flow. The LFP was found to increase to 400°C (the limit of the experimental setup), as compared to 370°C on the micropillar-covered surface.

In addition to coating the microstructures with nanoparticles, other techniques have also been applied to produce micro/nanoscale hierarchical surfaces. Kruse et al. [69] employed femtosecond laser surface processing (FLSP) technique to manufacture multiscale micro/nanostructured surfaces to tune the LFP. Three types of surface morphologies were fabricated: nanostructure-covered pyramids (NC-pyramids), below-surface-growth mounds (BSG-mounds) and above-surface-growth mounds (ASG-mounds), as depicted in Fig. 20(a). The size and shape of the microscale surface features were controlled through the laser fluence and the number of laser shots per area on the sample. Figure 20(b) shows the presence of self-assembled nanoparticles on top of the microstructures. Remarkable shifts in the LFP, as great as 175°C relative to the one on the polished surface, were observed (Fig. 20(c)). The greatest LFP increase was seen on NC-pyramid structures, which are characterized by 14 μm tall surface features separated by 25 μm that were blanketed with a thick layer of nanoparticles. Overall, the shift in the LFP was attributed to reduction in contact angle, capillary wicking and heterogeneous nucleation due to nanoporosity during the intermittent contact established by the microstructures. Using traditional anodic oxidation method, Lee et al. [70] prepared a multiscale micro/nanotextured surface (MTS) and compared the LFT on a polished surface (PS), a micro-rough surface (MRS) and the MTS sample. As shown in Fig. 21(a), the MTS structure is featured by nanoneedles of tens of nanometers in diameter with micron-size gaps. It was postulated that the low thermal capacity of the porous surface layer allows rapid cooling of the surface upon contact with the droplet, thus leading to the formation of a long-standing liquid precursor on the MTS. This capillary wicking induced liquid-solid contact then warrantees the LFP enhancement on the MTS, i.e., approximately 150°C and 120°C over that on the PS and the MRS (Fig. 21(b)).

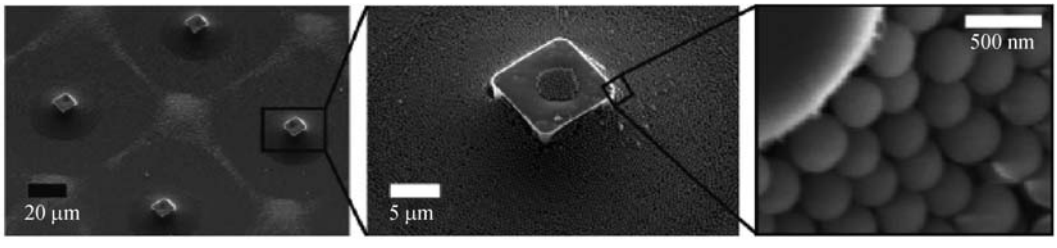

Fig. 19 Micro-nano hierarchical surface structure with micropillar array coated with nanoparticles (Adapted with permission from Kwon et al. [57])

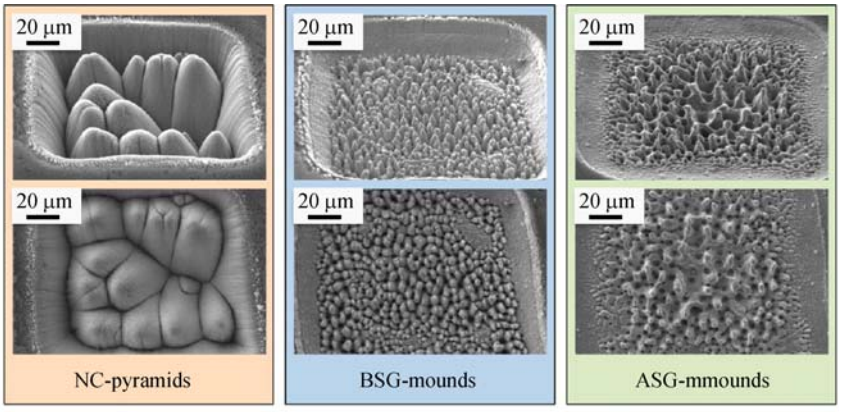

(a)

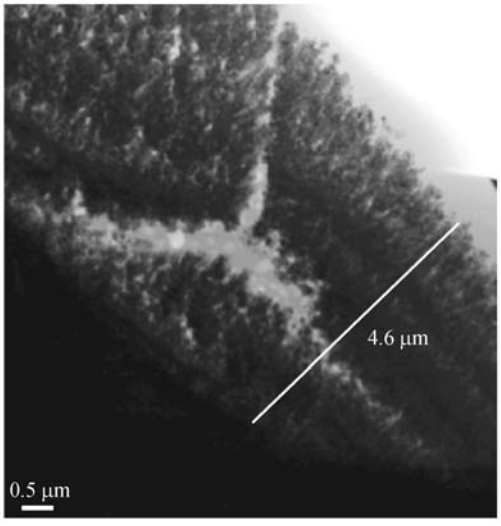

(b)

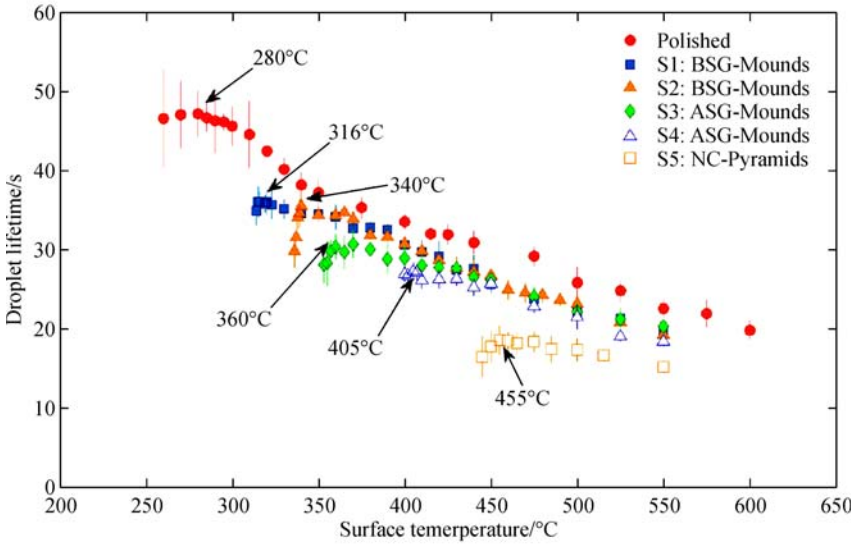

(c)

Fig. 20 Study of LFP on micro/nanoscale hierarchical surface

(a) FLSP-fabricated micro/nanoscale hierarchical surface structures; (b) transmission electron microscopy (TEM) images of self-assembled nanoparticles on the NC-pyramid structure; (c) droplet lifetime measurement with varying surface structures (Adapted with permission from Kruse et al. [69])

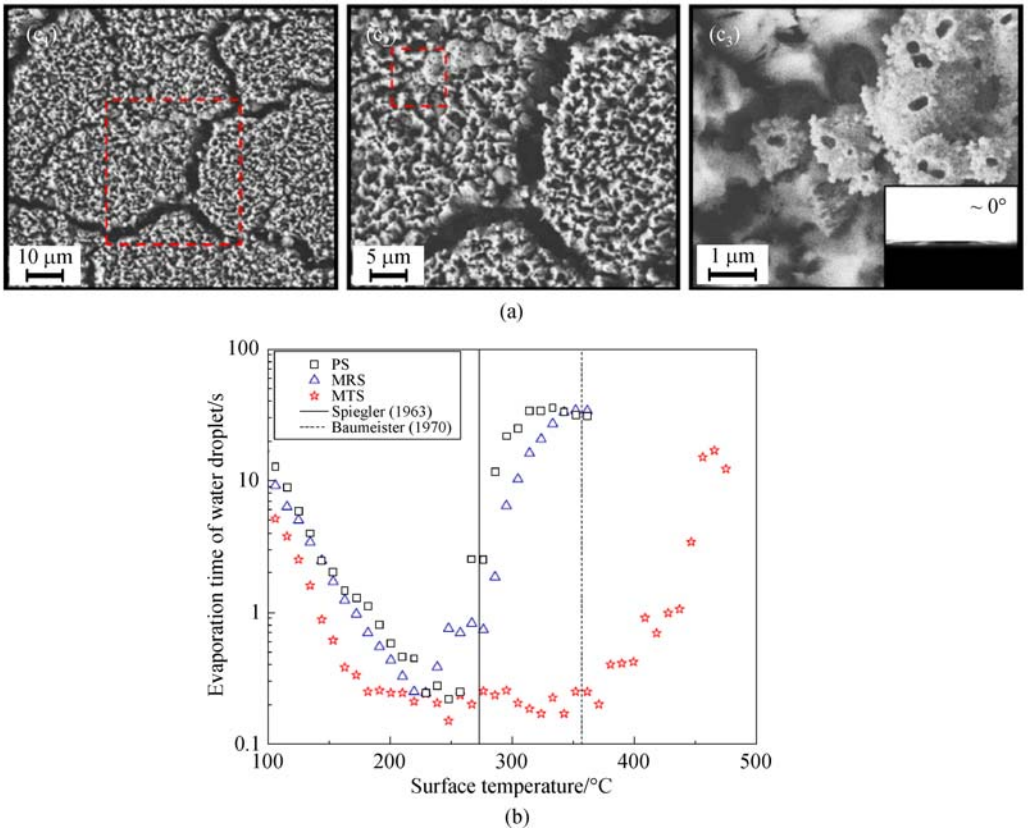

Fig. 21 Study of LFP on multiscale textured surface (MTS)
(a) SEM images of the MTS; (b) droplet lifetime on a polished surface, a micro-rough surface (MRS) and a MTS sample (Adapted with permission from Lee et al. [70])

The present design of most hierarchical LFP enhancement structures targets at utilizing microscale extrusion elements to establish the liquid-solid contact and, on top of them, creating a nanoporous layer by nanoparticles to promote capillary wicking and heterogeneous boiling. Essentially, the capillary wetting and the vapor escape share the same pathway. An alternative approach was recently developed by Farokhnia et al. [71] which employs a multiscale hierarchical topography to decouple the routes for the two competing processes. As shown in Fig. 22(a), the new structure consists of a superhydrophilic nanomembrane on the top of a high-aspect-ratio silicon micropillar array. The nanomembrane enforces wetting and keeps the droplet in contact with the solid surface. The generated vapor then enters the deep micropillar structure and flows out radially. Following the same rationale as in Ref. [57], the capillary force depends on the pore dimensions in the nanomembrane while the dewetting force is a function of the dimensions of the microstructure. Thus, independent control of the two forces can be achieved by accurately tailoring the dimensions of both the micro- and nanostructures. The experimental data in Fig. 22(b) indicate that the enhancement in LFP far exceeds those reported for other state-of-the-art hierarchical structures and, in fact, no LFP was observed at a temperature as high as 570°C.

3.2 Effect of porous structures on the Leidenfrost temperature

The use of porous surfaces to augment the Leidenfrost temperature is not new. For heat transfer surfaces with naturally grown micron-sized pores, it has been long postulated that vapor evaporated from the Leidenfrost droplet can be absorbed by or percolated in the porous matrix, thus helping to suppress the Leidenfrost effect. Avedisian and Koplik [24] was among the first to report a study of Leidenfrost droplets on porous/ceramic surfaces. The measured LFPs were 443 K, 570 K and 546 K for the polished stainless steel surface and the porous surfaces with 10% and 25% porosity, respectively. It was also observed the surface porosity results in a decrease in the droplet evaporation time due to a reduction in the vapor film thickness. To explain the positive correspondence of the LFP with porosity, a one-dimensional (1D) analytical model was constructed to derive the vapor film evolution for different surface porosities and wall temperature. The Brinkman extension of Darcy's law was applied to solve

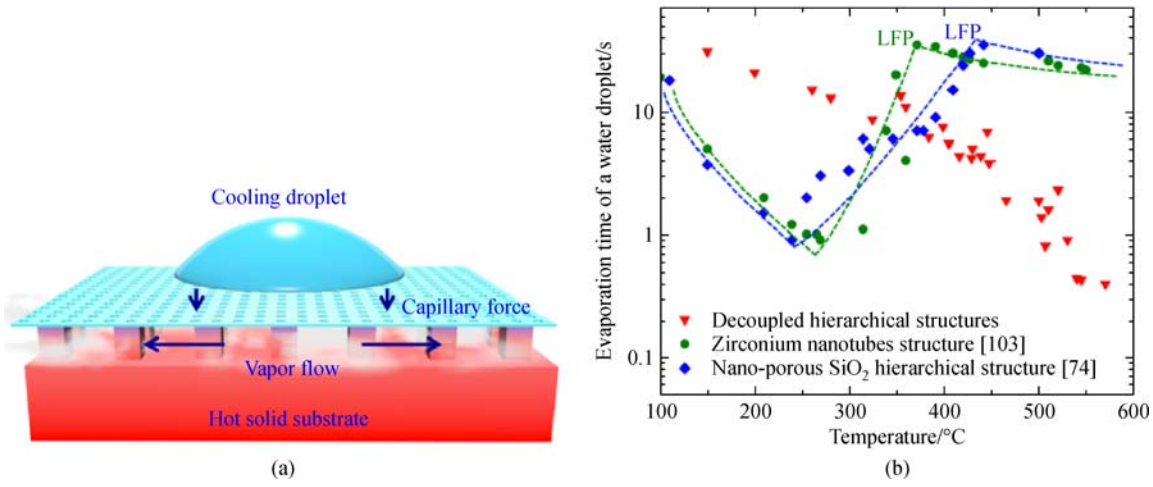

Fig. 22 Study of LFP on decoupled hierarchical surface for LFP enhancement
(a) Schematic of the surface structure; (b) droplet lifetime measurement on various micro/nanoscale hierarchical surfaces (Adapted with permission from Farokhnia et al. [71])

for the flow field inside the porous matrix, and a heuristic boundary condition was imposed at the interface between the vapor film and the porous layer to represent the balance of the shear stress on the fluid at the interface. This model was then improved by Fatehi and Kaviany [72] to resolve the contradiction between the predicted momentum boundary layer thickness that is smaller than a pore size and the elementary representative volume that must encompass a large number of pores to ensure a continuum treatment of the solid and fluid phases by a single momentum equation. Instead of the 1D model, a Beavers-Joseph semi-empirical boundary condition was used to predict the reduction in the vapor film thickness with respect to variations in permeability and thickness of the porous layer. Later, another work was presented by Chabičovský et al. [73] on the effects of porous oxide layer on the LFP during spray cooling of steel at high temperatures. The experimental and numerical simulation results confirm that the effective Leidenfrost temperature increases with increased oxide layer thickness and porosity.

In contrast, the effect of micro/nanoporous surfaces on the Leidenfrost phenomenon and the corresponding mechanisms remain explicit only till recently. As discussed in the previous section, micro/nanoporosity is believed to induce strong capillary wicking and act as nucleation sites to trigger explosive heterogeneous boiling, both beneficial to boosting the FLP. Since these micro/nanoporous features are often used together with the microscale surface features, their standalone effect on the Leidenfrost drop is somewhat elusive. Yu et al. [74] explored the water droplet impact on a porous surface in the Leidenfrost regime. The α-Al_2O_3 powders were deposited onto the substrate to yield a porosity of 34% and a pore size of 76 nm.The collision dynamics of the droplet (the droplet shape, spreading factor and height) was studied, and a three-dimensional (3-D) numerical model was developed to account for the transport phenomenon both inside and outside the porous media, by coupling the flow field with the heat and mass transfer process. The results reveal that the induced pressure in the vapor film is reduced and the droplet becomes less stable on the porous surface. Hu et al. [75] fabricated an anodized aluminum oxide (AAO) nanoporous surface and evaluated the enhancement of the cryogenic quenching heat transfer of liquid nitrogen by this surface. As shown in Fig. 23(a), the nanopores are approximately 50 nm in diameter and 5 μm in depth, and are arranged in a hexagonal pattern. The nanoporous surface demonstrates super hydrophilic properties. The liquid-vapor interface evolution on normal (smooth) and nanoporous surfaces in Fig. 23(b) depicts that the vapor film on the nanoporous surface is much thinner and contains less dynamic fluctuations. The experimental results in Fig. 23(c) also show an increase in the Leidenfrost temperature (32 K, or 25%) on the nanoporous surface, which was attributed to the enhanced wettability.

Geraldi et al. [76] presented a different approach to create microporous surface by weaving metal wires into a mesh. As shown in Fig. 24, the stainless steel mesh is a plain weave with square open areas between the wires and with each weft wire pasting alternatively over and under each warp wire. By using wires of different diameter and separation distance between wires, the mesh morphology can be varied. It was observed that the meshes elevate the Leidenfrost temperature to 315°C and the enhancement is proportional to the open area ratio. The shift of the FLP was attributed to the decrease of the contact area between the droplet and meshes as the open area becomes larger, thus requiring higher temperature to vaporize the liquid to form a stable vapor film. Most recently, a hierarchical micro/nanoporous structure was devised by Sajadi et al. [77] that demonstrates high heat dissipation capacity with

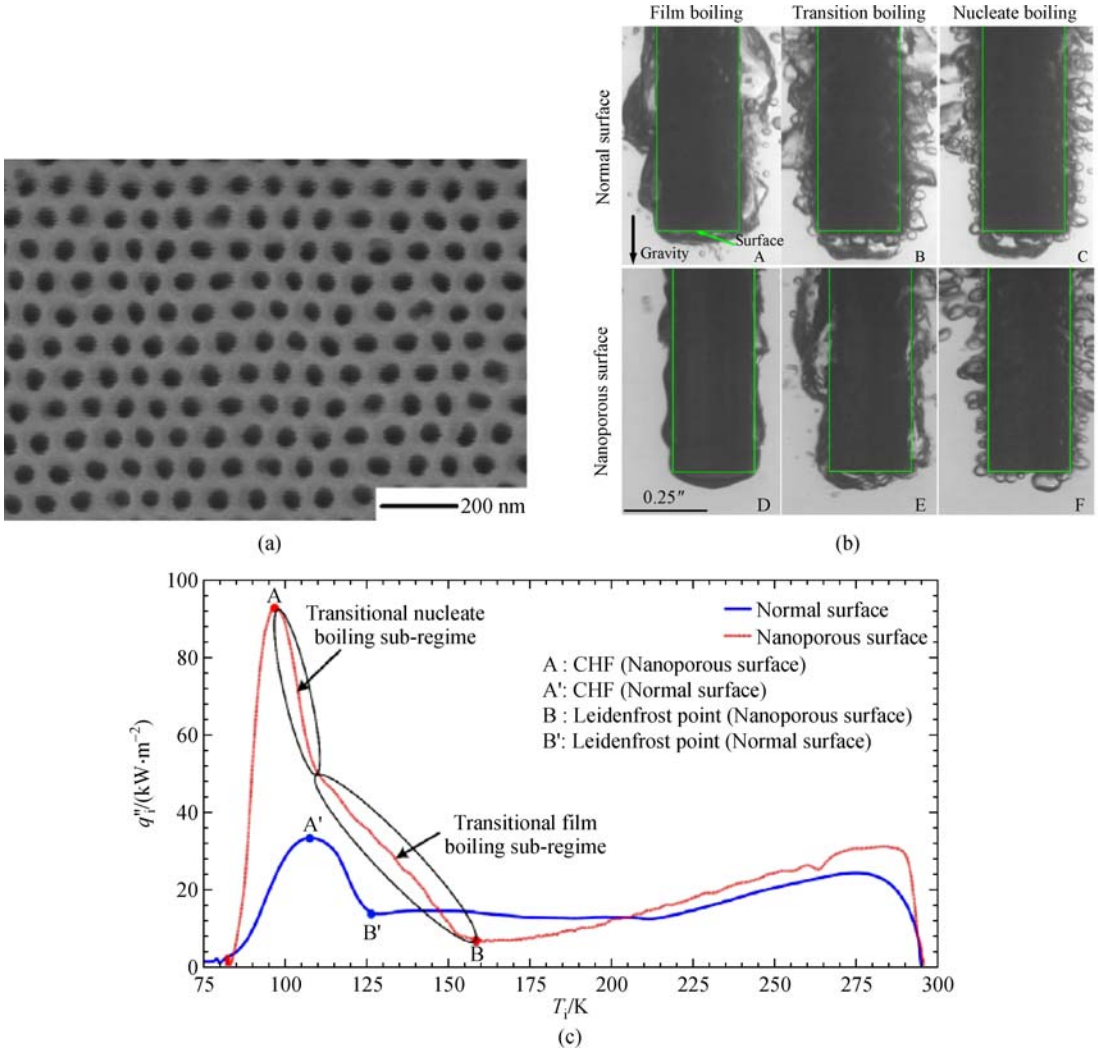

Fig. 23 Study of LFP on nanoporous surface

(a) SEM image of nanoporous surface; (b) comparison of boiling patterns on smooth and nanoporous surfaces; (c) comparison of heat flux for nanoporous surface and conventional surfaces during quenching (Adapted with permission from Hu et al. [75])

virtually no Leidenfrost limit. This structure was featured by a stack of two layers of corrugated Cu meshes with dimensions of 200 μm and 75 μm, which serves the role of micro capillars in providing the pathway for vapor flow. Copper nanoparticles of a cascade of different sizes, 425 μm, 75 μm and 60–80 nm, were then deposited on the stack of Cu meshes in sequence to form a nanoporous surface, as shown in Fig. 25(a). The Cu hierarchical structure works in a similar manner as for the Si decoupled structure [70] by independently controlling the capillary wetting force and the vapor dewetting force. Experiments conducted with Novec 7100 liquid (boiling temperature: 75°C) showed that nucleate boiling persists in all temperature ranges up to 225°C (as depicted in Fig. 25 (b)). Another additional attribute of this Leidenfrost suppression structure is that it can be manufactured in a one-step fabrication procedure with no need for micro/nanofabrication.

4 Concluding remarks

In this paper, a comprehensive review is provided with regard to the basic theories of the Leidenfrost phenomenon and the recent progress in the Leidenfrost temperature enhancement enabled by micro/nanoscale surface structuring. Overall, the general observations in the literature reveal that surface topology has a profound impact on the Leidenfrost phenomenon, and microscale and nanoscale surface features play different roles in affecting the Leidenfrost temperature. The microstructures are capable of re-establishing intermittent liquid-solid contact whereas nanoscale structures can promote liquid spreading and capillary wicking. However, when used alone, both the micro- and nanoscale surface structures exhibit some drawbacks or limitations, e.g., microstructures may adversely deteriorate the Leidenfrost point (LFP) due to the excessive generation of vapor or blockage of the

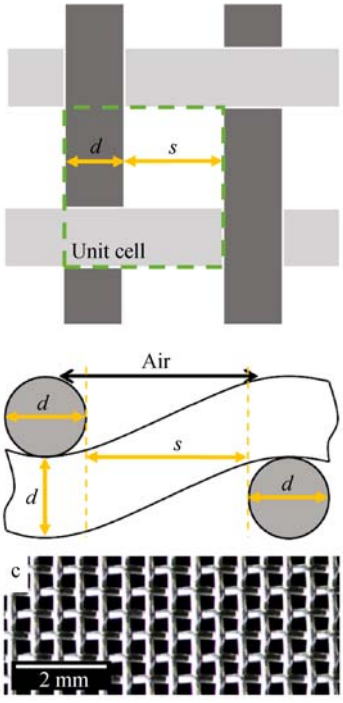

Fig. 24 Illustration of a metal mesh (Adapted with permission from Geraldi et al. [76])

vapor escape pathway and nanoscale structures mainly improves surface porosity. Therefore, the best practice for LFP enhancement appears to be from the multiscale hierarchical surfaces that combine the advantages of both length scales.

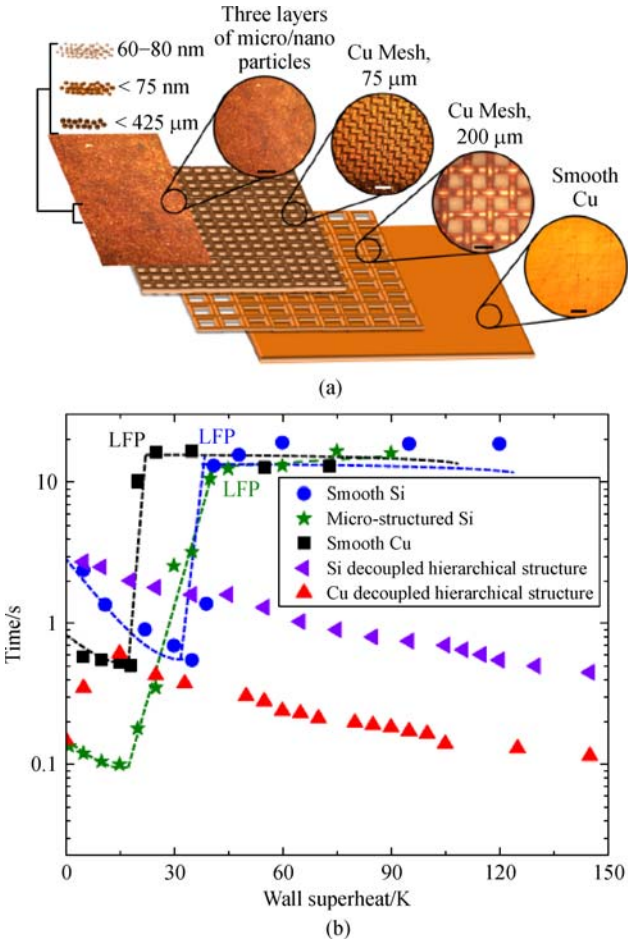

Fig. 25 Study of LFP on Cu hierarchical surface structure (a) Schematic of the Cu surface that consists of a stack of two corrugated Cu meshes and multi-layer of micro- and nanoparticles; (b) the evaporation time measurements of a Novec 7100 droplet on various surfaces where the Cu hierarchical surface exhibits no Leidenfrost limit (Adapted with permission from Sajadi et al. [77])

References

1. Leidenfrost J G. On the fixation of water in diverse fire. International Journal of Heat and Mass Transfer, 1966, 9(11): 1153–1166
2. Hall D D, Mudawar I, Morgan R E, Ehlers S L. Validation of a systematic approach to modeling spray quenching of aluminum alloy extrusions, composites, and continuous castings. Journal of Materials Engineering and Performance, 1997, 6(1): 77–92
3. Rein M. Interactions between drops and hot surfaces. In: Rein M. Drop-Surface Interactions. Vienna: Springer, 2002, 456: 185–217
4. Vorster W J J, Schwindt S A, Schupp J, Korsunsky A M. Analysis of the spray field development on a vertical surface during water spray-quenching using a flat spray nozzle. Applied Thermal Engineering, 2009, 29(7): 1406–1416
5. Zhang Y, Jia M, Liu H, Xie M, Wang T. Investigation of the characteristics of fuel adhesion formed by spray/wall interaction under diesel premixed charge compression ignition (PCCI) relevant conditions. Atomization and Sprays, 2015, 25(11): 933–968
6. Liang G T, Mudawar I. Review of drop impact on heated walls. International Journal of Heat and Mass Transfer, 2017, 106: 103–126
7. Gottfried B S, Bell K J. Film boiling of spheroidal droplets. Leidenfrost phenomenon. Industrial & Engineering Chemistry Fundamentals, 1966, 5(4): 561–568
8. Bernardin J D, Mudawar I. The Leidenfrost point: experimental study and assessment of existing models. Journal of Heat Transfer, 1999, 121(4): 894–903
9. Emmerson G S. The effect of pressure and surface material on the Leidenfrost point of discrete drops of water. International Journal of Heat and Mass Transfer, 1975, 18(3): 381–386
10. Kandlikar S G, Steinke M E. Contact angles and interface behavior during rapid evaporation of liquid on a heated surface. International Journal of Heat and Mass Transfer, 2002, 45(18): 3771–3780
11. Takata Y, Hidaka S, Cao J M, Nakamura T, Yamamoto H, Masuda M, Ito T. Effect of surface wettability on boiling and evaporation. Energy, 2005, 30(2–4): 209–220
12. Vakarelski I U, Patankar N A, Marston J O, Chan D Y C, Thoroddsen S T. Stabilization of Leidenfrost vapour layer by textured superhydrophobic surfaces. Nature, 2012, 489(7415): 274–277
13. Quéré D. Wetting and roughness. Annual Review of Materials

Research, 2008, 38(1): 71–99
14. Bradfield W S. Liquid-solid contact in stable film boiling. Industrial & Engineering Chemistry Fundamentals, 1966, 5(2): 200–204
15. Kim H, Buongiorno J, Hu L W, McKrell T. Nanoparticle deposition effects on the minimum heat flux point and quench front speed during quenching in water-based alumina nanofluids. International Journal of Heat and Mass Transfer, 2010, 53(7–8): 1542–1553
16. Zhong L, Guo Z. Effect of surface topography and wettability on the Leidenfrost effect. Nanoscale, 2017, 9(19): 6219–6236
17. Ko Y S, Chung S H. An experiment on the breakup of impinging droplets on a hot surface. Experiments in Fluids, 1996, 21(2): 118–123
18. Naber J D, Farrell P V. Hydrodynamics of droplet impingement on a heated surface. SAE Technical Paper, 1993, 930919
19. Quéré D. Leidenfrost dynamics. Annual Review of Fluid Mechanics, 2013, 45(1): 197–215
20. Mahadevan L, Pomeau Y. Rolling droplets. Physics of Fluids, 1999, 11(9): 2449–2453
21. Johnson K L. Contact Mechanics. New York: Cambridge University Press, 1987
22. Aussillous P, Quéré D. Properties of liquid marbles. Proceedings of the Royal Society of London A: Mathematical, Physical and Engineering Sciences, 2006, 462(2067): 973–999
23. Gottfried B S, Lee C J, Bell K J. Leidenfrost phenomenon-film boiling of liquid droplets on a flat plate. International Journal of Heat and Mass Transfer, 1966, 9(11): 1167–1188
24. Avedisian C T, Koplik J. Leidenfrost boiling of methanol droplets on hot porous/ceramic surfaces. International Journal of Heat and Mass Transfer, 1987, 30(2): 379–393
25. Biance A L, Clanet C, Quéré D. Leidenfrost drops. Physics of Fluids, 2003, 15(6): 1632–1637
26. Snoeijer J H, Brunet P, Eggers J. Maximum size of drops levitated by an air cushion. Physical Review. E, Statistical, Nonlinear, Biological and Soft Matter Physics 2009, 79(3): 036307
27. Burton J C, Sharpe A L, van der Veen R C A, Franco A, Nagel S R. Geometry of the vapor layer under a Leidenfrost drop. Physical Review Letters, 2012, 109(7): 074301
28. Snezhko A, Ben Jacob E, Aranson I S. Pulsating-gliding transition in the dynamics of levitating liquid nitrogen droplets. New Journal of Physics, 2008, 10(4): 043034
29. Holter N J, Glasscock W R. Vibrations of evaporating liquid drops. Journal of the Acoustical Society of America, 1952, 24(6): 682–686
30. Paul G, Manna I, Das P K. Formation, growth, and eruption cycle of vapor domes beneath a liquid puddle during Leidenfrost phenomena. Applied Physics Letters, 2013, 103(8): 084101
31. Ma X, Liétor-Santos J J, Burton J C. Star-shaped oscillations of Leidenfrost drops. Physical Review Fluids, 2017, 2(3): 031602
32. Tamura Z, Tanasawa Y. Evaporation and combustion of a drop contacting with a hot surface. Symposium (International) on Combustion, 1958, 7(1): 509–522
33. Tran T, Staat H J J, Prosperetti A, Sun C, Lohse D. Drop impact on superheated surfaces. Physical Review Letters, 2012, 108(3): 036101
34. Tran T, Staat H J J, Susarrey-Arce A, Foertsch T C, van Houselt A, Gardeniers H, Prosperetti A, Lohse D, Sun C. Droplet impact on superheated micro-structured surfaces. Soft Matter, 2013, 9(12): 3272–3282
35. Rein M. Drop-surface Interactions. Viena: Springer, 2002
36. Yagov V V, Lexin M A, Zabirov A R, Kaban'kov O N. Film boiling of subcooled liquids. Part I: Leidenfrost phenomenon and experimental results for subcooled water. International Journal of Heat and Mass Transfer, 2016, 100: 908–917
37. Liang G, Mudawar I. Review of spray cooling–Part 2: high temperature boiling regimes and quenching applications. International Journal of Heat and Mass Transfer, 2017, 115: 1206–1222
38. Baumeister K J, Simon F F. Leidenfrost temperature—its correlation for liquid metals, cryogens, hydrocarbons, and water. Journal of Heat Transfer, 1973, 95(2): 166–173
39. Liang G, Mudawar I. Review of drop impact on heated walls. International Journal of Heat and Mass Transfer, 2017, 106: 103–126
40. Berenson P J. Film-boiling heat transfer from a horizontal surface. Journal of Heat Transfer, 1961, 83(3): 351–356
41. Zuber N. On the stability of boiling heat transfer. Transactions of the American Society of Mechanical Engineers, 1958, 80: 711–716
42. Yao S C, Henry R E. An investigation of the minimum film boiling temperature on horizontal surfaces. Journal of Heat Transfer, 1978, 100(2): 260–267
43. Spiegler P, Hopenfeld J, Silberberg M, Bumpus C F Jr, Norman A. Onset of stable film boiling and the foam limit. International Journal of Heat and Mass Transfer, 1963, 6(11): 987–989
44. Schroeder-Richter D, Bartsch G. The Leidenfrost phenomenon caused by a thermo-mechanical effect of transition boiling: a revisited problem of non-equilibrium thermodynamics. Fundamentals of Phase Change: Boiling and Condensation, 1990, 13–20
45. Olek S, Zvirin Y, Elias E. The relation between the rewetting temperature and the liquid-solid contact angle. International Journal of Heat and Mass Transfer, 1988, 31(4): 898–902
46. Segev A, Bankoff S G. The role of adsorption in determining the minimum film boiling temperature. International Journal of Heat and Mass Transfer, 1980, 23(5): 637–642
47. Bernardin J D, Mudawar I. A cavity activation and bubble growth model of the Leidenfrost point. Journal of Heat Transfer, 2002, 124 (5): 864–874
48. Ahn H S, Jo H J, Kang S H, Kim M H. Effect of liquid spreading due to nano/microstructures on the critical heat flux during pool boiling. Applied Physics Letters, 2011, 98(7): 071908
49. Dong L, Quan X, Cheng P. An experimental investigation of enhanced pool boiling heat transfer from surfaces with micro/nanostructures. International Journal of Heat and Mass Transfer, 2014, 71 (4): 189–196
50. Bernardin J D, Stebbins C J, Mudawar I. Effects of surface roughness on water droplet impact history and heat transfer regimes. International Journal of Heat and Mass Transfer, 1996, 40(1): 73–88
51. Bernardin J D, Mudawar I. A Leidenfrost point model for impinging droplets and sprays. Journal of Heat Transfer, 2004, 126(2): 272–278
52. Elbahri M, Paretkar D, Hirmas K, Jebril S, Adelung R. Anti-lotus effect for nanostructuring at the Leidenfrost temperature. Advanced Materials, 2007, 19(9): 1262–1266
53. Cui Q, Chandra S, McCahan S. The effect of dissolving salts in

water sprays used for quenching a hot surface: Part 2—spray cooling. Journal of Heat Transfer, 2003, 125(2): 333–338
54. Abdalrahman K H M, Sabariman, Specht E. Influence of salt mixture on the heat transfer during spray cooling of hot metals. International Journal of Heat and Mass Transfer, 2014, 78(7): 76–83
55. Huang C K, Carey V P. The effects of dissolved salt on the Leidenfrost transition. International Journal of Heat and Mass Transfer, 2007, 50(1): 269–282
56. Kim H, Truong B, Buongiorno J, Hu L W. On the effect of surface roughness height, wettability, and nanoporosity on Leidenfrost phenomena. Applied Physics Letters, 2011, 98(8): 083121
57. Kwon H M, Bird J C, Varanasi K K. Increasing Leidenfrost point using micro-nano hierarchical surface structures. Applied Physics Letters, 2013, 103(20): 201601
58. Feng R, Wu X, Xue Q. Profile characterization and temperature dependence of droplet control on textured surfaces. Chinese Science Bulletin, 2011, 56(18): 1930–1934
59. Arnaldo del Cerro D, Marín Á G, Römer G R B E, Pathiraj B, Lohse D, Huis in't Veld A J. Leidenfrost point reduction on micropatterned metallic surfaces. Langmuir, 2012, 28(42): 15106–15110
60. Park I W, Fernandino M, Dorao C A. Effect of micropillar characteristics on Leidenfrost temperature of impacting droplets. In: Proceedings of ASME 14th International Conference on Nanochannels, Microchannels and Minichannels, Washington, USA, 2016
61. Hays R, Maynes D, Crockett J. Thermal transport to droplets on heated superhydrophobic substrates. International Journal of Heat and Mass Transfer, 2016, 98: 70–80
62. Nair H, Staat H J J, Tran T, van Houselt A, Prosperetti A, Lohse D, Sun C. The Leidenfrost temperature increase for impacting droplets on carbon-nanofiber surfaces. Soft Matter, 2014, 10(13): 2102–2109
63. Weickgenannt C M, Zhang Y, Sinha-Ray S, Roisman I V, Gambaryan-Roisman T, Tropea C, Yarin A L. Inverse-Leidenfrost phenomenon on nanofiber mats on hot surfaces. Physical Review. E, Statistical, Nonlinear, Biological, and Soft Matter Physics, 2011, 84 (3): 036310
64. Weickgenannt C M, Zhang Y, Lembach A N, Roisman I V, Gambaryan-Roisman T, Yarin A L, Tropea C. Nonisothermal drop impact and evaporation on polymer nanofiber mats. Physical Review. E, Statistical, Nonlinear, Biological, and Soft Matter Physics , 2011, 83(3): 036305
65. Sinha-Ray S, Zhang Y, Yarin A L. Thorny devil nanotextured fibers: the way to cooling rates on the order of 1 kW/cm^2. Langmuir, 2011, 27(1): 215–226
66. Kim S H, Ahn H S, Kim J, Kaviany M, Kim M H. Dynamics of water droplet on a heated nanotubes surface. Applied Physics Letters, 2013, 102(23): 233901
67. Auliano M, Fernandino M, Zhang P, Dorao C A.The Leidenfrost phenomenon on silicon nanowires. In: Proceeding ASME 2016 14th International Conference on Nanochannels, Microchannels, and Minichannels, Washington, USA, 2016
68. Agapov R L, Boreyko J B, Briggs D P, Srijanto B R, Retterer S T, Collier C P, Lavrik N V. Asymmetric wettability of nanostructures directs Leidenfrost droplets. ACS Nano, 2014, 8(1): 860–867
69. Kruse C, Anderson T, Wilson C, Zuhlke C, Alexander D, Gogos G, Ndao S. Extraordinary shifts of the Leidenfrost temperature from multiscale micro/nanostructured surfaces. Langmuir, 2013, 29(31): 9798–9806
70. Lee G C, Kang J Y, Park H S, Moriyama K, Kim S H, Kim M H. Induced liquid-solid contact via micro/nano multiscale texture on a surface and its effect on the Leidenfrost temperature. Experimental Thermal and Fluid Science, 2017, 84: 156–164
71. Farokhnia N, Sajadi S M, Irajizad P, Ghasemi H. Decoupled hierarchical structures for suppression of Leidenfrost phenomenon. Langmuir: the ACS Journal of Surfaces & Colloids, 2017, 33(10): 2541–2550
72. Fatehi M, Kaviany M. Analysis of levitation of saturated liquid droplets on permeable surfaces. International Journal of Heat and Mass Transfer, 1990, 33(5): 983–994
73. Chabičovský M, Hnízdil M, Tseng A A, Raudenský M. Effects of oxide layer on Leidenfrost temperature during spray cooling of steel at high temperatures. International Journal of Heat and Mass Transfer, 2015, 88: 236–246
74. Yu Z, Wang F, Fan L S. Experimental and numerical studies of water droplet impact on a porous surface in the film-boiling regime. Industrial & Engineering Chemistry Research, 2008, 47(23): 9174–9182
75. Hu H, Xu C, Zhao Y, Shaeffer R, Ziegler K J, Chung J N. Modification and enhancement of cryogenic quenching heat transfer by a nanoporous surface. International Journal of Heat and Mass Transfer, 2015, 80(5): 636–643
76. Geraldi N R, McHale G, Xu B, Wells G G, Dodd L E, Wood D, Newton M I. Leidenfrost transition temperature for stainless steel meshes. Materials Letters, 2016, 176: 205–208
77. Sajadi S M, Irajizad P, Kashyap V, Farokhnia N, Ghasemi H. Surfaces for high heat dissipation with no Leidenfrost limit. Applied Physics Letters, 2017, 111(2): 021605